International Journal of Computational Methods


# Dispersion-preserving implicit-explicit numerical methods for reactive flow models

Emmanuel A. Amikiya * and Mapundi K. Banda

*Department of Mathematics and Applied Mathematics,*
*University of Pretoria, Private Bag X20,*
*Hatfield 0028, South Africa*
*amixaddsmall@yahoo.com*

Received (Day Month Year)
Revised (Day Month Year)

Chemical reactions occur everywhere in both natural and artificial systems. Some of the reactions occur during the flow of a fluid (such a process is referred to as a reactive flow). Given the hazardous nature of some reactive flows, computer simulations (rather than physical experiments) are necessary for ascertaining or enhancing our understanding of such systems. The process of simulation involves mathematical and numerical modelling of the reactive flows. Mathematical models for reactive flow problems are complicated partial differential equations that often lack exact solutions, thus, numerical solutions are employed. Numerical methods must preserve almost all the relevant properties of the problem for accuracy reasons. Dispersion relations are important properties of wave propagation problems and numerical methods that satisfy them are called dispersion preserving methods. Furthermore, stiff transport models are wave propagation problems that cannot be solved efficiently with explicit methods. However fully implicit methods are computationally expensive. A combination of implicit and explicit methods called implicit-explicit methods are usually employed to efficiently resolve stiffness. An example of problems of interest in this regard are the advection-diffusion-reaction (ADR) models. In this discussion, spectral analysis is performed on two implicit-explicit methods to ascertain their dispersion preserving abilities in order to determine their suitability for simulating general stiff reactive flow problems. The analysis shows that both implicit-explicit methods are dispersion preserving, however, one particular method is more suitable for general wave propagation problems.

*Keywords*: Reactive flow, Spectral analysis, Dispersion relations, Wave propagation problems, Implicit-explicit methods

## 1. Introduction

Dispersion is a phenomenon where waves of different frequencies travel at different speeds. The concept of dispersion plays a crucial role in a wide range of scientific and engineering applications that involve wave propagation. It has been investigated extensively in electromagnetic wave propagation problem (see for example

*Ghana Institute of Management and Public Administration, Achimota, Greater Accra, GHANA.

[ Álvarez-Pérez *et al.* (2019)] and [Li *et al.* (2018)]), acoustics (see for example [Palermo *et al.* (2019)] and [Song *et al.* (2021)]) and in the area of optics (see for example [Hassanien *et al.* (2020)] and [Hassanien and Sharma (2020)]). In most of the extant literature, dispersion is used to characterise real physical wave propagation problems through physical experiments and measurements. However, the present work employs dispersion to characterise numerical solution procedures that are developed for the simulation of reactive flow. Real physical experiments are not always possible for reactive flows due to the cost and hazardous nature of some reactive flow. Under such circumstances, computer simulations are employed to enhance understanding of the systems. The simulations involve mathematical modelling and numerical simulations.

Mathematical models for reactive flow phenomena are parabolic/hyperbolic partial differential equations that describe advection, diffusion and reaction (ADR) processes. The models describe the propagation of waves and are characteristically non-linear [Djouad and Sportisse (2003)], composed of large systems of equations (i.e. have high degrees of freedom, see [Amikiya and Banda (2018)] for further information), usually characterised by stiffness due to disparate reaction rates. Among the models, advection-diffusion-reaction models are common and cover a wide area of applications (see for example [Sun *et al.* (2023); Tripathi and Bhupendra (2020); Wang *et al.* (2019); Luo *et al.* (2019); Zhang and Decheng (2019)]) in the broad disciplines of engineering, biology and thermodynamics. Such models will be considered in this discussion.

Further, due to complications in the model, it is not always possible to obtain exact concentration profiles for the chemical species [Benito and Hristo (2013); Suman *et al.* (2017); Amikiya and Banda (2018)]. An alternative to finding exact solutions is developing numerical methods. Solutions obtained with numerical methods are approximations to the exact solution, thus, accuracy depends on the ability of the method to closely mimic the chemistry and physics described by the governing equation [Suman *et al.* (2017)]. Thus the numerical methods must preserve the natural properties of the natural phenomenon which they are approximating. The efficiency of such schemes is also paramount. It is necessary to develop highly accurate numerical methods as alternatives to the exact solution. This requires rigorous error analysis of the numerical method for a particular problem. However, the non-availability of exact solutions make numerical analysis difficult and sometimes impossible without simplifying assumptions. Models are often linearised first, and then followed by analyses to obtain analytical relations (e.g. exact solutions, dissipation and dispersion expressions), which are relevant for analysing numerical methods [Suman *et al.* (2017)]. There are many techniques for analysing numerical methods, the common techniques include Taylor expansions (used to obtain consistency of the method), von Neumann stability analysis [Trefethen (1982); Strikwerda (2004)], Gustafsson, Kreiss, Sundstrom (GKS) stability theory [Gustafsson *et al.* (1972)] and time-stability analysis [Carpenter *et al.* (1993); Zhong (1998)].

Analysis performed in a full spectral domain yields stability, dispersion and dissipation information about the governing equations [Sengupta (2013)]. However, the traditional techniques of numerical analysis have limitations when applied in full domain spectral analysis [Suman *et al.* (2017)]. In addition, the approximative nature of the numerical approaches, spurious properties such as artificial oscillations may be observed in the numerical solutions.

Traditionally, errors are quantified by measuring numerical solutions relative to the exact solution, however, dispersion/dissipation relations are more appropriate for quantifying errors in propagation problems. Numerical schemes that satisfy dispersion relations for a particular propagation problem are said to be Dispersion-Relation-Preserving (DRP) schemes. Dispersion relations obtained for a propagation problem vary across various analyses. Due to the limitations of the Von Neumann (and other listed techniques), Global Spectral Analysis has gained popularity in research involving propagation problems [Sengupta *et al.* (2017); Sengupta (2013); Sengupta *et al.* (2009); Sengupta *et al.* (2009)].

The authors in [Sengupta *et al.* (2003)] have analysed numerical schemes for the linear advection equation by adapting the Spectral Analysis approach presented in [Vichnevetsky and Bowles (1982)]. By performing spectral analysis on the linear advection equation, the authors in [Sengupta *et al.* (2007)] have shown that numerical methods have different error and signal dynamics. Finite Difference Schemes for linear diffusion equation have been analysed in [Sengupta and Bhole (2014)]. One notable observation in the linear advection and diffusion cases is that, numerical phase speed and numerical coefficient of diffusion are not constant. Positivity-preserving Galerkin method for advection-diffusion-reaction have also been analysed in [Joshi and Jaiman (2017)] using the spectral approach. In [Sengupta *et al.* (2012)] spectral analysis of Galerkin finite element method for the advection equation have been discussed. One observation with the finite element methods is good error dispersion behaviour.

Furthermore, compact finite difference and finite volume methods for Euler equations have been discussed in [Sengupta *et al.* (2005)]. The compact finite difference methods proved superior in the resolution of Riemann problems. Finite difference methods for Navier-Stokes equations have been analysed by traditional techniques in [Sousa (2001); Kwok (1992); Chan (1984); Wesseling (1996)]. In [Suman *et al.* (2017)], the authors extended the spectral approach to compact finite difference methods for linear advection-diffusion equation in order to ascertain accurate schemes for the Navier-Stokes equations.

In this discussion, we consider models with a reactive term. We first derive dispersion relations for reactive flow models by performing spectral analysis of the linear ADR equation. Next, we present and analyse two implicit-explicit numerical methods for reactive transport problems in order to ascertain their suitability for general chemical transport models that are characteristically stiff. Due to high degrees of freedom, stiffness and positivity constraints associated with chem-

ical transport problems, not all numerical methods are suitable [Blom and Verwer (2000); Verwer *et al.* (2004); David *et al.* (2004); Anna *et al.* (2003)]. Fully implicit methods are suitable for resolving stiffness [Djouad and Sportisse (2003); McRae and Seinfeld (2000); Zhang *et al.* (1998)] however, such methods are expensive to implement. An efficient numerical approach to resolving stiff problems is the implicit-explicit approach, where implicit methods are applied to the stiff part and explicit methods are employed for the non-stiff part [Christopher and Mark (2001); Verwer *et al.* (2004)]. Further, in addition to low cost in computational time, implicit-explicit methods possess properties of both explicit and fully implicit methods, thus, have broader application area. Suitable implicit-explicit methods must be Dispersion-Relation-Preserving. Thus, dispersion relations (derived by performing spectral analysis on the linear model) are used to analyse the implicit-explicit methods (with WENO and central differencing discretisation of the space derivatives). Although a scalar linear model is considered in the analysis, we will show later that results are not limited but apply to systems, multi-space dimensions, semi- and fully nonlinear transport problems.

The aim of this work is to analyse and characterise efficient and suitable computational methods for simulating reactive flows. The numerical procedures and analysis presented here are novel, thus, the work contributes to the literature on numerical simulation of wave propagation problems. The discussion here achieves the goal in six sections. In Section 2, the unknown concentration variable and linear transport equation are transformed to spectral variables and equations, respectively. Followed by a discussion on the exact dispersion relations. In Section 3, the numerical methods are presented, followed by a discussion on the numerical dispersion relations for the implicit-explicit methods. In Section 4, suitability (i.e. consistency and stability) analyses with regards to the normalised dispersion relation are presented. In Section 5, numerical experiments are conducted to confirm the analysis and verify the numerical methods. Finally, the discussion is concluded in Section 6.

## 2. Dispersion relations of 1D advection-diffusion-reaction equation

Chemical transport phenomena involves physical processes (such as advection and diffusion) and chemical reactions. Consider a prototype model such as a linear 1D advection-diffusion-reaction equation given by:

$$\frac{\partial U}{\partial t} + u\frac{\partial U}{\partial x} = \Gamma\frac{\partial^2 U}{\partial^2 x} + K_r U, \tag{1}$$

where $U$ denotes concentration of a chemical species, $x$ is a space variable, $t$ is a time variable, $u$ denotes constant transport velocity, $K_r$ is chemical reactivity and $\Gamma$ denotes constant diffusivity. Three special cases of the linear equation (1) occur when the reactivity, $K_r$, takes the values zero, positive or negative. Thus Equation (1) models pure diffusion (non-reactive), diffusion-destruction and diffusion-production when the reactivity $K_r$ takes the values zero, negative or positive, respectively.

The exact dispersion relations for the linear transport equation are firstly determined by applying global spectral analysis. Thus, by transforming the concentration function $U(x,t)$, from the $x-t$ plane to the hybrid spectral plane [Sengupta (2013); Sengupta *et al.* (2003); Johnson (1997)], we obtain:

$$U(x,t) = \int \mathcal{U}(\kappa,t) e^{i\kappa x} d\kappa, \tag{2}$$

where $\mathcal{U}(\kappa,t)$ is the Fourier amplitude and $\kappa$ is the wave number. Using the spectral transform (2), the linear chemical transport model (1) can be represented in the spectral plane as:

$$\frac{\partial \mathcal{U}}{\partial t} + iu\kappa\mathcal{U} = -\Gamma\kappa^2\mathcal{U} + K_r\mathcal{U}, \tag{3}$$

Given a general initial condition $U(x,0) = \int \mathcal{U}_0(\kappa) e^{i\kappa x} d\kappa$, the exact solution of (3) can be obtained as follows:

$$\mathcal{U}(\kappa,t) = \mathcal{U}_0(\kappa) e^{-(i\kappa u + \kappa^2\Gamma - K_r)t}. \tag{4}$$

Moreover, the concentration of the chemical species can also be represented in the bi-dimensional Fourier-Laplace transform:

$$U(x,t) = \iint \mathcal{U}(\kappa,\omega) e^{i(\kappa x - \omega t)} d\kappa\, d\omega, \tag{5}$$

where $\omega$ denotes circular frequencies. Applying the Fourier-Laplace transform (5) directly in the linear convection-diffusion-reaction equation (1), yields the physico-chemical dispersion relation:

$$\omega = u\kappa - i(\kappa^2\Gamma - K_r). \tag{6}$$

Wave propagation problems are characterised by dispersion relations, that yield information about the phase and group velocities of propagating signals [Johnson (1997)]. Any numerical algorithm for solving a wave propagation problem can only be suitable/accurate if it satisfies the dispersion relation for the problem under consideration [Sengupta (2013); Sengupta *et al.* (2007)]. In [Sengupta *et al.* (2017)], multiple time level schemes have been analysed based on correct dispersion relations for convection problems and in [Suman *et al.* (2017)], the idea has been adapted for convection-diffusion problems. In this discussion, the same idea will be used to analyse the linear chemical transport problem.

Denote the time step size by $\Delta t$, spatial step size by $\Delta x$, Peclet number by $P_e = \frac{\Gamma\Delta t}{\Delta x^2}$, Courant-Friedrich-Lewis (CFL) number by $C_f = \frac{u\Delta t}{\Delta x}$, $\lambda_r = K_r\Delta t$, and the physico-chemical amplification factor by $G_{\text{ex}}$. The amplification factor of the exact solution is defined as follows:

$$G_{\text{ex}} = \frac{\mathcal{U}(\kappa, t+\Delta t)}{\mathcal{U}(\kappa,t)} \tag{7}$$

Using the analytical solution (4) in definition (7) yields the following physical-chemical amplification factor:

$$G_{\text{ex}} = e^{-(i\kappa u + \kappa^2 \Gamma - K_r)\Delta t}. \tag{8}$$

Using Peclet and CFL number relations, the amplification factor (8) can be re-expressed as follows:

$$\begin{aligned} G_{\text{ex}} &= e^{-i\omega\Delta t} \\ &= e^{-P_e(\kappa\Delta x)^2 + \lambda_r} e^{-iC_f(\kappa\Delta x)}. \end{aligned} \tag{9}$$

Further, if numerical approximations are applied to the advection and diffusion derivatives after substituting (2) into the advection-diffusion reaction equation, a semi-discrete equation is obtained as follows:

$$\frac{\partial \mathcal{U}}{\partial t} + iu\kappa_{\text{adv}}\mathcal{U} = -\Gamma\kappa_{\text{dif}}^2\mathcal{U} + K_r\mathcal{U}, \tag{10}$$

where $\kappa_{\text{adv}}$ and $\kappa_{\text{dif}}^2$ are functions of $\kappa$ resulting from the numerical approximations of the advection and diffusion derivatives, respectively. The functions $\kappa_{\text{adv}}$ and $\kappa_{\text{dif}}^2$ represent numerical wave numbers for advection and diffusion, respectively.

The analytical solution of the semi-discrete equation (10) with initial data $U(x,0) = \int \mathcal{U}_0(\kappa)e^{i\kappa x}\, d\kappa$ is given by:

$$\mathcal{U}_{\text{apx}}(\kappa, t) = \mathcal{U}_0(\kappa)e^{-(iu\kappa_{\text{adv}} + \Gamma\kappa_{\text{dif}}^2 - K_r)t}. \tag{11}$$

Using the numerical solution (11) in definition (7) yields the following numerical amplification factor:

$$G_{\text{apx}} = e^{-(P_e(\kappa_{\text{dif}}\Delta x)^2 - \lambda_r)} e^{-iC_f(\kappa_{\text{adv}}\Delta x)}. \tag{12}$$

Another expression relating numerical diffusion wave number $\kappa_{\text{dif}}$, with the magnitude of the amplification factor can be obtained from (12) as follows:

$$\Big(\frac{\kappa_{\text{dif}}}{\kappa}\Big)^2 = \frac{\lambda_r - \ln|G_{\text{apx}}|}{P_e(\kappa\Delta x)^2}. \tag{13}$$

According to the numerical amplification factor (13), the shift in phase for each time step is given by:

$$\phi = \kappa_{\text{adv}} u \Delta t, \tag{14}$$

and is related to the amplification factor by the expression:

$$\tan(\phi) = -\Big(\frac{\text{Im}(G_{\text{apx}})}{\text{Re}(G_{\text{apx}})}\Big), \tag{15}$$

where $\text{Im}(G_{\text{apx}})$ and $\text{Re}(G_{\text{apx}})$ denote the imaginary and real parts of the amplification factor $G_{\text{apx}}$, respectively.

A normalized numerical advection wave number $\kappa_{\text{adv}}$ related to the amplification factor is obtained from (14) and (15) as follows:

$$\frac{\kappa_{\text{adv}}}{\kappa} = -\frac{1}{C_f(k\Delta x)} \arctan\Big(\frac{\text{Im}(G_{apx})}{\text{Re}(G_{\text{apx}})}\Big). \tag{16}$$

The normalized quantities (13) and (16) for a particular numerical method when evaluated will be one if the method has the same numerical diffusion and advection wave numbers as the exact solution. Highly accurate numerical methods for the time-dependent advection-diffusion-reaction problem must have ratios close to one.

In the next section the numerical discretisation for the differential equations using the method of lines are introduced. The spectral operators are introduced and discussed.

## 3. Implicit-Explicit methods

The method of lines is introduced. For time discretisation the Implicit-Explicit Methods are introduced. Further for the spatial discretisation, the Weighted Essentially Non-Oscillatory (WENO) scheme will be employed.

### 3.1. *Temporal discretisation*

Method of lines procedure enable the conversion of a partial differential equation (PDE) into an ordinary differential equation (ODE) [Blom and Verwer (2000)]. In general, an autonomous time-dependent ODE states that, find $\mathcal{U}$ such that:

$$\frac{\partial \mathcal{U}}{\partial t} = F(\mathcal{U}), \tag{17}$$

subject to some initial conditions.

A combination of implicit and explicit discretisation procedures popularly called IMEX discretisation yields efficient schemes for many problems including reactive transport problems [Shu (1997)]. In this procedure the slope function $F(\mathcal{U})$ is expressed as a sum of several other functions and then explicit procedures are applied to non-stiff functions and implicit procedures are applied to stiff functions. The ODE for the simplest case where the slope function is the sum of two functions, states that:

$$\frac{\partial \mathcal{U}}{\partial t} = G(\mathcal{U}) + H(\mathcal{U}), \tag{18}$$

where $H(\mathcal{U})$ denotes the non-stiff part and $G(\mathcal{U})$ denotes the stiff part. The non-stiff term in the 1D linear reactive problem under consideration is the advection term and the diffusion-reaction terms are considered stiff.

Thus one IMEX scheme (named IMEX-FBE1) for solving ODE (18) states that:

$$\mathcal{U}^{n+1} = \mathcal{U}^n + \Delta t\Big(G(\mathcal{U}^{n+1}) + H(\mathcal{U}^n)\Big) \tag{19}$$

Applying the above approach to (3) yields the following functions:

$$H(\mathcal{U}) = -iu\kappa_{\text{adv}}\mathcal{U}, \quad G(\mathcal{U}) = (-\kappa_{\text{dif}}^2\Gamma + K_r)\mathcal{U}. \tag{20}$$

The IMEX-FBE1 method for the 1D linear problem can be re-written as:

$$(1-P)\mathcal{U}^{n+1} = (1 - iC_f\kappa_{\text{adv}}\Delta x)\mathcal{U}^n, \tag{21}$$

where $P = -P_e(\kappa_{\text{dif}}\Delta x)^2 + \lambda_r$.

Thus, the amplification factor for IMEX-FBE1 is given by:

$$G_{\text{FBE1}} = \frac{1}{1-P} - i\frac{C_f\kappa_{\text{adv}}\Delta x}{1-P}. \tag{22}$$

Another IMEX scheme (named IMEX-FBE2) for solving the ODE (18) states that:

$$\begin{aligned} \mathcal{U}^* &= \mathcal{U}^n + \Delta t\Big(G(\mathcal{U}^*) + H(\mathcal{U}^n)\Big) \\ \mathcal{U}^{n+1} &= \mathcal{U}^n + \Delta t\Big(G(\mathcal{U}^*) + H(\mathcal{U}^*)\Big) \end{aligned} \tag{23}$$

Using fluxes (20) in expressions (23) yields the IMEX-FBE2 method:

$$\begin{aligned} (1-P)\mathcal{U}^* &= (1 - iC_f\kappa_{\text{adv}}\Delta x)\mathcal{U}^n \\ \mathcal{U}^{n+1} &= \mathcal{U}^n + (P - iC_f\kappa_{\text{adv}}\Delta x)\mathcal{U}^* \end{aligned} \tag{24}$$

Thus, the amplification factor for IMEX-FBE2 is given by:

$$G_{\text{FBE2}} = \frac{1-(C_f\kappa_{\text{dif}}\Delta x)^2}{1-P} - i\frac{C_f\kappa_{\text{adv}}\Delta x(1+P)}{1-P}. \tag{25}$$

### 3.2. *Spatial discretisation*

Oscillations from inaccurate discretisation of the advection term could result in negative concentration values which have no physical meaning. Weighted essentially non-oscillatory (WENO) discretisations are very efficient for resolving such oscillations [Shu (1997)]. The third order finite difference WENO is considered here. Denote the linear advective flux in (1) by $f(U) = uU$, then a conservative finite difference approximation at the $i^{th}$ spatial node $x_i$, is given by [Shu (1997)]:

$$\frac{\partial}{\partial x}f|_{x_i} \approx \frac{1}{\Delta x}\Big(\hat{f}_{i+\frac{1}{2}} - \hat{f}_{i-\frac{1}{2}}\Big), \tag{26}$$

where $\hat{f}_{i+\frac{1}{2}}$ denotes a numerical flux evaluated at interface $x_{i+\frac{1}{2}}$. The third order WENO reconstruction of the numerical flux is given by [Shu (1997); Tian and Yong-Tao (1982)]:

$$\hat{f}_{i+\frac{1}{2}} = w_0\Big(\frac{1}{2}f(U_i) + \frac{1}{2}f(U_{i+1})\Big) + w_1\Big(-\frac{1}{2}f(U_{i-1}) + \frac{3}{2}f(U_i)\Big), \tag{27}$$

where

$$w_r = \frac{\alpha_r}{\alpha_1+\alpha_2}, \quad \alpha_r = \frac{d_r}{(\epsilon+\beta_r)^2}, \quad r = 0, 1,$$

the linear weights are $d_0 = \frac{2}{3}$, $d_1 = \frac{1}{3}$, the smoothness indicators are $\beta_0 = \Big[f(U_{i+1}) - f(U_i)\Big]^2$, $\beta_1 = \Big[f(U_i) - f(U_{i-1})\Big]^2$ and $\epsilon = 10^{-3}$ is a parameter taken to ensure a non-zero denominator.

Applying the numerical flux (27) in approximation (26) yields:

$$\frac{\partial}{\partial x}f|_{x_i} \approx \frac{w_1}{2\Delta x}f_{i-2} - \frac{(4w_1+w_0)}{2\Delta x}f_{i-1} + \frac{3w_1}{2\Delta x}f_i + \frac{w_0}{2\Delta x}f_{i+1}. \tag{28}$$

WENO discretisations assume optimal order when the nonlinear weights become linear, thus, the following analysis assumes that the WENO approximation (28) is optimal (i.e. $w_0 = \frac{2}{3}$ and $w_1 = \frac{1}{3}$). Using the linear flux in (28), transforming into spectral variables (using (2)) and manipulating algebraically yields:

$$\begin{aligned}\kappa_{\text{adv}}\Delta x = &\frac{-w_1\sin(2\kappa\Delta x) + (4w_1+2w_0)\sin(\kappa\Delta x)}{2} \\ &- i\frac{w_1\cos(2\kappa\Delta x) - 4w_1\cos(\kappa\Delta x) + 3w_1}{2}\end{aligned} \tag{29}$$

The derivative corresponding to diffusion is discretised using the second order central differencing approximation as follows:

$$\Gamma\frac{\partial^2 U}{\partial x^2}|_{x_i} \approx \frac{\Gamma}{(\Delta x)^2}\Big(U_{i+1} - 2U_i + U_{i-1}\Big). \tag{30}$$

Transforming (30) into spectral variables (by applying (2)) and manipulating algebraically yields:

$$(\kappa_{\text{dif}}\Delta x)^2 = 2 - 2\cos(\kappa\Delta x). \tag{31}$$

Therefore, the physico-chemical amplifications for IMEX-FBE1 and IMEX-FBE2 are defined by (22) and (25), respectively, using expressions (29) and (31). Normalised dispersion relations (i.e. Equation (13), Equation (16) and the amplification ratios) for both schemes are derived by applying the numerical schemes' amplification factors (22) and (25), in Equation (16).

In the next section the numerical dispersion relations are discussed. Consideration is first made for the preservation of the amplification relation. Thereafter, the preservation of the diffusion relation is discussed followed by the preservation of the advection relation and a comparative discussion is undertaken.

## 4. Dispersion analysis of the IMEX schemes

In this section, dispersion analysis is performed on the IMEX schemes presented in Section 3. Consistency and stability information of each scheme are obtained under three dispersion conditions (i.e. amplification factor, wave number diffusion and wave number advection) and under three reactive flow categories. Consistency and stability details of IMEX-FBE1 and IMEX-FBE2 are computed for different Peclet numbers, CFL numbers, reaction conditions, and wave numbers. Contours of normalised amplification factors, diffusion and advection wave numbers of the IMEX methods are presented in Figures 1-6. A numerical method is consistent with regards to a dispersion relation if the range of values for a particular normalised relation,

evaluated for a numerical method contains a one (1). Further, the numerical method is unstable if the range of values for a particular normalised relation evaluated for any numerical method involves negative numbers. In the case of instability, the region of instability is the area between the minimum value and zero.

### 4.1. *Preservation of amplification relation*

In the diffusion-production flow regime, normalised amplification factor for IMEX-FBE1 method increases in the closed interval $[0.01, 3.88]$ when $P_e = 0.05$ (see Figure 1a) and $[0.03, 6.41]$ when $P_e = 0.25$ (see Figure 2a) across CFL and wave numbers. The normalised amplification factor for IMEX-FBE2 increases in the closed interval $[0, 135.03]$ when $P_e = 0.05$ (see Figure 1b) and $[0, 324.03]$ when $P_e = 0.25$ (see Figure 2b) across CFL and wave numbers. The observations here imply that both methods are consistent and stable with regards to normalised amplification factor, however, IMEX-FBE1 has better damping capabilities.

In the diffusion-destruction model, the normalised amplification factor for IMEX-FBE1 method increases in the closed interval $[0.01, 4.17]$ when $P_e = 0.05$ (see Figure 1c) and $[0.04, 8.83]$ when $P_e = 0.25$ (see Figure 1d) across CFL and wave numbers. The normalised amplification factor for IMEX-FBE2 increases in the closed interval $[0, 161.16]$ when $P_e = 0.05$ (see Figure 2c) and $[0, 446.21]$ when $P_e = 0.25$ (see Figure 2d) across CFL and wave numbers. The observations here imply that both methods are consistent and stable.

In the non-reactive model, the normalised amplification factor for IMEX-FBE1 method increases in the closed interval $[0.01, 3.96]$ when $P_e = 0.05$ (see Figure 1e) and $[0.03, 7.52]$ when $P_e = 0.25$ (see Figure 2e) across CFL and wave numbers. The normalised amplification factor for IMEX-FBE2 increases in the closed interval $[0, 146.6]$ when $P_e = 0.05$ (see Figure 1f) and $[0, 379.94]$ when $P_e = 0.25$ (see Figure 2f) across CFL and wave numbers. These observations imply that both methods are consistent and stable.

### 4.2. *Preservation of diffusion relation*

In the diffusion-production model, normalised numerical diffusion relation for IMEX-FBE1 method increases in the closed interval $[-4.6297E11, 6.26]$ when $P_e = 0.05$ (see Figure 3a) and $[-9.2594E10, 1.53]$ when $P_e = 0.25$ (see Figure 4a) across CFL and wave numbers. The normalised diffusion relation for IMEX-FBE2 increases in the closed interval $[-4.6293E11, 3.04]$ when $P_e = 0.05$ (see Figure 3b) and $[-9.2587E10, 3.04]$ when $P_e = 0.25$ (see Figure 4b) across CFL and wave numbers. The observation here imply that both methods are consistent and conditionally stable with regards to normalised diffusion relation. However, IMEX-FBE2 is more stable than IMEX-FBE1 due to its relatively smaller region of instability.

In the diffusion-destruction model, normalised numerical diffusion wave number for IMEX-FBE1 method increases in the closed interval $[-3.5367E11, 6.04]$ when $P_e = 0.05$ (see Figure 3c) and $[-7.0734E10, 1.45]$ when $P_e = 0.25$ (see Figure 4c)

across CFL and wave numbers. The normalised diffusion relation for IMEX-FBE2 increases in the closed interval $[-3.5371E11, 3.04]$ when $P_e = 0.05$ (see Figure 3d) and $[-7.0742E10, 2.96]$ when $P_e = 0.25$ (see Figure 4d) across CFL and wave numbers. The observations imply that both methods are consistent and conditionally stable with regards to normalised diffusion relation. In contrast with the diffusion-production case, IMEX-FBE1 is more stable due to its relatively smaller region of instability.

In the non-reactive model, normalised diffusion relation for the IMEX-FBE1 method increases in the closed interval $[-9.8696E7, 6.16]$ when $P_e = 0.05$ (see Figure 3e) and $[-1.9739E7, 1.49]$ when $P_e = 0.25$ (see Figure 4e) across CFL and wave numbers. The normalised diffusion relation for IMEX-FBE2 increases in the closed interval $[-9.8695E7, 13.74]$ when $P_e = 0.05$ (see Figure 3f) and $[-1.9739E7, 2.96]$ when $P_e = 0.25$ (see Figure 4f) across CFL and wave numbers. The observations imply that both methods are consistent and conditionally stable with regards to normalised diffusion relation. IMEX-FBE2 is more stable than IMEX-FBE1 due to its relatively smaller region of instability.

### 4.3. *Preservation of advection relation*

In all flow regimes, normalised advection relation for the IMEX-FBE1 method increases in the closed interval $[-1, 0.7]$ when $P_e = 0.05$ and $[-1, 0.7]$ when $P_e = 0.25$ across CFL and wave numbers. The normalized advection relation for IMEX-FBE2 increases in the closed interval $[-2.62, 2.61]$ when $P_e = 0.05$ and $[-2.62, 2.61]$ when $P_e = 0.25$ across CFL and wave numbers. These observations are shown in Figures 5 and 6. The observations here imply that both methods are consistent and conditionally stable. Further, IMEX-FBE1 has a smaller region of instability thus, it is more stable than IMEX-FBE2.

### 4.4. *Discussion of results*

The results presented in the subsections above imply that, in the simulation of a diffusion-production reactive flow system where chemical reactions result in the increase in concentration of a species, both IMEX schemes are able to preserve the amplification relation. However, IMEX-FBE1 preserves the advection relation better due to its narrower region of instability. IMEX-FBE2 preserves the diffusion relation better than IMEX-FBE1, due to its narrower region of instability.

Further, the results also imply that in the simulation of a diffusion-destruction reactive flow system, both IMEX methods preserve the amplification relation. However, IMEX-FBE1 preserve advection and diffusion due to its narrower region of instability.

Finally, the results imply that in the simulation of a non-reactive flow system, both IMEX schemes are able to preserve the amplification relation. However, IMEX-FBE1 preserves the advection relation better due to its narrower region of

instability. IMEX-FBE2 preserves the diffusion relation better than IMEX-FBE1, due to its narrower region of instability.

In general, IMEX-FBE1 is more suitable for all the flow regimes due to its consistency and narrower region of stability. In the simulation of systems that are dominated by diffusion, IMEX-FBE2 can be deployed due to its ability to preserve the diffusion relation.

In the next section, further analysis is undertaken in which the IMEX schemes are applied to different models (equations) possess the dispersion property.

## 5. Numerical experiments

In this section the findings in the previous section are further applied to three examples: a 1D system, a 1D nonlinear problem, a 2D problem as well as an environmental chemical reaction example.

### 5.1. *Experiments in spectral plane*

The exact solution for the ODE (3) can be expressed in terms of the Peclet and wave numbers as follows:

$$\mathcal{U}(\kappa, t^n) = \mathcal{U}_0(\kappa) e^{-n(iC_f \kappa \Delta x + P_e(\kappa \Delta x)^2 - \lambda_r)}, \tag{32}$$

where the $n^{th}$ time gridpoint is given by $t^n = n\Delta t$. The solutions of the recurrence relations (19) and (23) can be written as:

$$\mathcal{U}^n = \mathcal{U}_0(\kappa) G^n_{\text{apx}}, \tag{33}$$

where $G_{\text{apx}}$ is given by $G_{\text{FBE1}}$ in (22) for IMEX-FBE1 or $G_{\text{FBE2}}$ in (25) for IMEX-FBE2.

Figures 7, 8 and 9 show comparisons of the analytical solution and numerical solutions obtained with the IMEX methods. In particular, Figures 7 and 8 show that under different Peclet, CFL and wave number values, IMEX-FBE1 has better damping properties than IMEX-FBE2. Figure 9 shows the superiority of IMEX-FBE1 over IMEX-FBE2 in all cases.

### 5.2. *Accuracy tests with 1D system*

The first 1D problem (with exact solution) considered for testing the accuracy of the IMEX schemes is a system (of two advection-diffusion transport equations with stiffness in the reaction part) that seeks to find $U(x,t)$ and $V(x,t)$ such that:

$$\frac{\partial U}{\partial t} + \frac{\partial uU}{\partial x} = \Gamma \frac{\partial^2 U}{\partial x^2} - K_u U + V, \qquad 0 < x < 2\pi, \tag{34}$$

$$\frac{\partial V}{\partial t} + \frac{\partial uV}{\partial x} = \Gamma \frac{\partial^2 V}{\partial x^2} - K_v V, \qquad 0 < x < 2\pi. \tag{35}$$

Using periodic boundary conditions, the exact solution for the system (34)-(35) is:

$$U(x,t) = \left(e^{-(K_u+\Gamma)t} + e^{-(K_v+\Gamma)t}\right)\cos(x-ut), \tag{36}$$

$$V(x,t) = (K_u - K_v)e^{-(K_v+\Gamma)t}\cos(x-ut). \tag{37}$$

The input data are as follows:

$$\Gamma = 0.01, \quad u = 0.01, \quad K_v = 1, \quad K_u = 100, \tag{38}$$

and the initial data are as follows:

$$U(x,0) = 2\cos(x), \tag{39}$$

$$V(x,0) = (K_u - K_v)\cos(x). \tag{40}$$

Figure 10, shows the solution and error profiles for IMEX-FBE1 and IMEX-FBE2 applied to the stiff system. It is clear that both numerical schemes are accurate and convergent for the stiff system. Table 1 shows that both schemes have the same order of convergence. Two finite difference schemes (that are order one and have been discussed in [Suman *et al.* (2017)]) have also been applied to solve this system. The first finite difference scheme is derived by applying forward-differencing to the time derivatives and central differencing to all spatial derivatives (this scheme is named Euler-CD2-CD2) and the second finite difference scheme is obtained by applying forward differencing to the time derivatives, forward differencing to advection terms and central differencing to diffusion terms (this scheme is named Euler-UP1-CD2). Figure 11, shows that the IMEX schemes are superior in accuracy to both finite difference schemes. The results in this test problem shows that the findings in the dispersion analyses are not limited to single transport equations.

### 5.3. *Accuracy tests with 1D nonlinear problem*

Secondly, a 1D reactive transport equation where all the processes (i.e. advection, diffusion and reaction) are nonlinear, is considered for testing the accuracy of the IMEX schemes. This fully nonlinear problem seeks to find $U(x,t)$ such that [Tian and Yong-Tao (1982)]:

$$\frac{\partial U}{\partial t} + \frac{\partial U}{\partial x} = \frac{\partial}{\partial x}U\frac{\partial U}{\partial x} - 1 - 0.25\cos(2(x-t)) + U, \qquad 0 < x < 2\pi. \tag{41}$$

With the initial condition $U(x,0) = 1+0.5\sin(x)$ and periodic boundary conditions, the analytical solution is:

$$U(x,t) = 1 + 0.5\sin(x-t). \tag{42}$$

Some computed solutions for this 1D fully nonlinear problem are displayed in Figure 12. The results show that the IMEX schemes (especially IMEX-FBE1) are

Table 1: Errors and orders ($L_\infty$) of the numerical schemes applied to solve system (34)-(35), errors were computed using analytical solution (37). The solutions and errors were computed for diffusion dominated, advection dominated and semi-linear transport cases using $\Delta t = 0.5\Delta x$.

| **Convergence test** | | | | | |
|---|---|---|---|---|---|
| Transport | Spatial steps ($N_x$) | IMEX-FBE1 | | IMEX-FBE2 | |
| | | Error | Order | Error | Order |
| Diffusion | 10 | 4.9012 | - | 4.9012 | - |
| | 20 | 2.8100 | 0.8026 | 2.8100 | 0.8026 |
| | 40 | 1.4371 | 0.9674 | 1.4371 | 0.9674 |
| | 80 | 0.7190 | 0.9991 | 0.7190 | 0.9991 |
| | 160 | 0.3660 | 0.9742 | 0.3660 | 0.9742 |
| Advection | 10 | 4.8363 | - | 4.8757 | - |
| | 20 | 2.7788 | 0.7994 | 2.7886 | 0.8060 |
| | 40 | 1.4103 | 0.9785 | 1.4129 | 0.9807 |
| | 80 | 0.7119 | 0.9862 | 0.7119 | 0.9889 |
| | 160 | 0.3568 | 0.9965 | 0.3568 | 0.9965 |
| Advection-diffusion | 10 | 4.9040 | - | 4.9436 | - |
| | 20 | 2.8065 | 0.8052 | 2.8166 | 0.8116 |
| | 40 | 1.4375 | 0.9652 | 1.4355 | 0.9724 |
| | 80 | 0.7192 | 0.9991 | 0.7192 | 0.9971 |
| | 160 | 0.3681 | 0.9663 | 0.3669 | 0.9710 |

accurate and have better stiffness resolution capabilities than the finite difference schemes. Results for this test problem indicate that the findings in the dispersion analyses are not limited to linear transport problems.

### 5.4. *Accuracy tests with 2D problems*

Furthermore, to show that the findings in the dispersion analyses are not limited to 1D problems, two 2D reactive transport problems are considered here for testing the accuracy of the schemes. The first problem is the 2D version of system (34)-(35) given by [Tian and Yong-Tao (1982)]:

$$\frac{\partial U}{\partial t} + \frac{u}{2}\Big(\frac{\partial U}{\partial x} + \frac{\partial U}{\partial y}\Big) = \frac{\Gamma}{2}\Big(\frac{\partial^2 U}{\partial x^2} + \frac{\partial^2 U}{\partial y^2}\Big) - K_u U + V, \qquad 0 < x, y < 2\pi, \quad (43)$$

$$\frac{\partial V}{\partial t} + \frac{u}{2}\Big(\frac{\partial V}{\partial x} + \frac{\partial V}{\partial y}\Big) = \frac{\Gamma}{2}\Big(\frac{\partial^2 V}{\partial x^2} + \frac{\partial^2 V}{\partial y^2}\Big) - K_v V, \qquad 0 < x, y < 2\pi. \quad (44)$$

With periodic boundary conditions, the exact solution is:

$$U(x,y,t) = \left(e^{-(K_u+\Gamma)t} + e^{-(K_v+\Gamma)t}\right)\cos(x+y-ut), \tag{45}$$

$$V(x,y,t) = (K_u - K_v)e^{-(K_v+\Gamma)t}\cos(x+y-ut). \tag{46}$$

The second 2D problem is fully nonlinear and its given by [Tian and Yong-Tao (1982)]:

$$\begin{aligned}\frac{\partial U}{\partial t} + 0.5\frac{\partial U^2}{\partial x} + 0.5\frac{\partial U^2}{\partial y} &= \frac{\partial}{\partial x}U\frac{\partial U}{\partial x} + \frac{\partial}{\partial y}U\frac{\partial U}{\partial y} - U^2 \\ &+ 1.125 - 0.625\cos(2(x+y-t)) + 0.25\sin(2(x+y-t)) \\ &+ 0.5\cos(x+y-t) + 2\sin(x+y-t), \qquad 0 < x, y < 2\pi. \end{aligned} \tag{47}$$

With periodic boundaries, the analytical solution is:

$$U(x,y,t) = 1 + 0.5\sin(x+y-t). \tag{48}$$

The results are displayed in Figure 13. Both IMEX schemes are efficient in resolving stiffness in the problem involving a system, while IMEX-FBE1 is better in the fully nonlinear case. The results here indicate that the findings in the dispersion analysis are not limited to 1D problems.

### 5.5. *Application: environmental chemical engineering system*

Acidic effluents from mineral mines have adverse ecological and health impact on receiving environments. One method for attenuating the acidity in effluents is limestone neutralisation. The acid-calcite reaction occur as follows [Werner and Lee*et al.* (1961); Ayora *et al.* (2013); Plummer *et al.* (1978); Reddy *et al.* (1981)]:

$$CaCO_3 + H^+ \rightleftharpoons Ca^{2+} + HCO_3^-, \tag{49}$$

$$CaCO_3 + H_2CO_3 \rightleftharpoons Ca^{2+} + 2HCO_3^-, \tag{50}$$

$$CaCO_3 + H_2O \rightleftharpoons Ca^{2+} + HCO_3^+ + OH^-. \tag{51}$$

Experimental data shows that reactions (50) and (51) contribute insignificantly compared with reaction (49), thus, the system reduces to reaction (49) which contains the chemical species [Amikiya and Banda (2018)]:

$$\mathbf{C} = \left(CaCO_3, H^+, Ca^{2+}, HCO_3^-\right),$$

whose corresponding concentrations (i.e. current and initial) and source/sink vectors are denoted by [Amikiya and Banda (2018)]:

$$\mathbf{U} = \left(U_1, U_2, U_3, U_4\right), \quad \mathbf{U}_0 = \left(U_{10}, U_{20}, U_{30}, U_{40}\right)$$

and

$$\mathbf{S} = \left(0, \quad -K_f U_2 + K_b U_3 U_4, \quad K_f U_2 - K_b U_3 U_4, \quad K_f U_2 - K_b U_3 U_4\right),$$

respectively, where $K_f$ and $K_b$ denote reaction constants.

Hydrogen ions ($k = 2$) are responsible for acidity of the effluent water, therefore, neutralisation of the hydrogen ions implies attenuation of the pollutant. Relevant system of semi-linear transport equations to solve for hydrogen ions is given by:

$$\frac{\partial \mathbf{U}}{\partial t} + \frac{\partial u\mathbf{U}}{\partial x} = \Gamma \frac{\partial^2 \mathbf{U}}{\partial x^2} + \mathbf{S}. \tag{52}$$

System (52) has four (i.e. high) degrees of freedom thus, is computationally expensive to solve since only hydrogen concentration (i.e. one degree of freedom) is required. A reduced semi-linear equation for hydrogen ions only (using the stoichiometric method in [Amikiya and Banda (2018)]) is given by:

$$\frac{\partial U_2}{\partial t} + \frac{\partial uU_2}{\partial x} = \Gamma \frac{\partial^2 U_2}{\partial x^2} + \alpha_{H1} U_2^2 + \alpha_{H2} U_2 + \alpha_{H3}, \tag{53}$$

where $\alpha_{H1} = K_b$, $\alpha_{H2} = -K_f + K_b\Big(2U_{20} + U_{40} + U_{30}\Big)$ and $\alpha_{H3} = K_b\Big(U_{10} + U_{40}\Big)\Big(U_{20} + U_{30}\Big)$.

Input data used in the numerical experiments are:

$$L_x = 2\pi,\ T = 1, u = 0.01, \Gamma = 0.01, K_f = 0.13,\ K_b = 0.0025, K_h = 1,$$
$$U_{20} = 0.01\cos(x),\ U_{30} = 0.0001\cos(x),\ U_{40} = 0.0001\cos(x).$$

Figure 14 shows the solutions of IMEX-FBE1 and IMEX-FBE2 (applied to solve both large and reduced models) in all the transport cases (i.e. advection, diffusion and advection-diffusion cases). It can be observed that the solution of both schemes are decreasing with time thus, reproducing the chemistry of neutralisation. Moreover, Figure 15, shows decreasing error profile for IMEX-FBE1 and increasing error profile for IMEX-FBE2, thus IMEX-FBE1 is more compatible with the model reduction procedure. Furthermore, CPU time given by Figure 16 shows that IMEX-FBE1 is less expensive to implement.

## 6. Conclusion

Suitable and efficient computational methods for reactive flows are those methods that preserve the dispersion relations as well as have low computational time. This work has presented and analysed two computational methods that are suitable and efficient for simulating reactive flow problems.

Firstly, normalised dispersion relations (amplification factor, diffusion and advection relations) for the linear advection-diffusion-reaction (a prototype of chemical transport models) were derived using global spectral analysis in Section 2. Followed by a discussion on the development of two implicit-explicit numerical methods (i.e. IMEX-FBE1 and IMEX-FBE2) for simulating reactive flow problems (see Section 3).

Secondly, the normalised dispersion relations (amplification factor, diffusion and advection relations) were deployed to analyse the two implicit-explicit numerical methods (i.e. IMEX-FBE1 and IMEX-FBE2), see Section 4. Analysis shows that both methods preserve amplification relation, however, IMEX-FBE2 preserves the diffusion relation better while IMEX-FBE1 preserves the advection relation better than IMEX-FBE2. In general, IMEX-FBE1 has better consistency than IMEX-FBE2 in all the three flow regimes considered.

Thirdly, numerical experiments were conducted to validate the analysis in Section 5. The results from the numerical experiments show that the IMEX schemes presented here are more accurate than some finite differencing schemes of the same order. The results also show that the IMEX schemes can resolve stiffness in fully nonlinear reactive flow problems. Further, the results show that the IMEX schemes can resolve multi-dimensional stiff reactive flow systems and are compatible with model reduction schemes. The results confirm that both schemes are efficient and suitable for chemical reactive flow problems but IMEX-FBE1 has better solution properties (i.e. more accurate and has low CPU time), as predicted by the dispersion analysis.

In conclusion, the schemes presented here are dispersion-preserving and are capable of efficiently simulating reactive flow problems. However, it is worth noting here that, IMEX-FBE1 is more efficient and thus, recommended for simulating general reactive flow problems.

## Acknowledgments

This work is part of a PhD thesis by EAA, University of Pretoria, South Africa. It was supported in part by the National Research Foundation of South Africa (Grant Number: 93476). Sincere gratitude to Prof. Francois Smit and Prof. Jules Djoko-Kamdem for the constructive criticism of this work. EAA also appreciates the support of GIMPA, Ghana.

## References

Álvarez-Pérez, Gonzalo, Voronin, Kirill V. and Volkov, Valentyn S. and Alonso-González, Pablo and Nikitin, Alexey Y. Analytical approximations for the dispersion of electromagnetic modes in slabs of biaxial crystals, Physical Review B 100 (2019)

Palermo, A., Wang, Y., Celli, P. and Daraio, C. Tuning of surface-acoustic-wave dispersion via magnetically modulated contact resonances. Physical Review Applied, 11(4) 2019, p.044057.

Song, Zhenghong, Xiangfang Zeng, and Clifford H. Thurber. "Surface-wave dispersion spectrum inversion method applied to Love and Rayleigh waves recorded by distributed acoustic sensing." Geophysics 86, no. 1 (2021): EN1-EN12.

Li, Xiong, Mingbo Pu, Xiaoliang Ma, Yinghui Guo, Ping Gao, and Xiangang Luo. "Dispersion engineering in metamaterials and metasurfaces." Journal of Physics D: Applied Physics 51, no. 5 (2018): 054002.

Hassanien Ahmed Saeed, Neffati R.,Aly K.A., Impact of Cd-addition upon optical properties and dispersion parameters of thermally evaporated CdxZn1-xSe films: Discussions

on bandgap engineering, conduction and valence band positions, Optik 212 (2020) 0030-4026

Hassanien Ahmed Saeed and Ishu Sharma, Optical properties of quaternary a-Ge15-x Sbx Se50 Te35 thermally evaporated thin-films: refractive index dispersion and single oscillator parameters, Optik 200 (2020) 0030-4026

Rafik Djouad and Bruno Sportisse, Solving reduced chemical models in air pollution modelling, Applied Numerical Mathematics 44 (2003) 49-61.

Benito M. C. and Hristo V. K., An unconditionally positivity preserving scheme for advection-diffusion reaction equations, Journal of Mathematical and Computer Modelling 57 (2013) 2177-2185.

Suman V.K., Sengupta T. K., Jyothi D. P. C., Surya M. K., Deepanshu S., Spectral analysis of finite difference schemes for convection diffusion equation, Computers and Fluids 150 (2017) 95-114.

Amikiya, A. E. and Banda, M.K., (2018). Modeling and simulation of reactive transport phenomena. Journal of computational science, 28, p.155-167.

Sun, Tiezhi, Zhi Zong, Yingjie Wei, and Guiyong Zhang. "Modeling and computation of unsteady cavitating flows involved thermal effects using partially averaged navier–stokes method." International Journal of Computational Methods 20, no. 08 (2023): 1850095.

Tripathi, Bhavya, and Bhupendra Kumar Sharma. "Influence of heat and mass transfer on two-phase blood flow with joule heating and variable viscosity in the presence of variable magnetic field." International Journal of Computational Methods 17, no. 03 (2020): 1850139.

Wang, Wenxin, Boyan Mao, Bao Li, Xi Zhao, Chensi Xu, Youjun Liu, and Jian Liu. "Numerical simulation of instantaneous wave-free ratio of stenosed coronary artery." International Journal of Computational Methods 16, no. 03 (2019): 1842009.

Luo, Ke, Wentao Jiang, Chen Yu, Xiaobao Tian, Zhihong Zhou, and Yuan Ding. "Fluid–solid interaction analysis on iliac bifurcation artery: a numerical study." International Journal of Computational Methods 16, no. 07 (2019): 1850112.

Zhang, Youlin, and Decheng Wan. "MPS-FEM coupled method for fluid–structure interaction in 3d dam-break flows." International Journal of Computational Methods 16, no. 02 (2019): 1846009.

Trefethen L. N., Group velocity in finite difference scheme. SIAM Rev 1982 24(2) 113-36.

Strikwerda J., Finite difference schemes and partial differential equations. 2nd ed. Society for Industrial and Applied Mathematics; 2004. doi: 10.1137/1. 9780898717938.

Gustafsson B, Kreiss H-O and Sundstrom A., Stability theory of difference approximations for mixed initial boundary value problems. II. Math Comput 1972 26 (119) 649-86 . URL http://www.jstor.org/stable/2005093.

Carpenter M. H., Gottlieb D.,and Abarbanel S., The stability of numerical boundary treatments for compact high-order finite-difference schemes. J Comput Phys 1993 108(2) 272-95. http://dx.doi.org/10.1006/jcph.1993.1182. URL http://www.sciencedirect.com/science/article/pii/S0021999183711824

Zhong X., High-order finite-difference schemes for numerical simulation of hypersonic boundary-layer transition. J Comput Phys 1998 144(2) 662-709. http://dx.doi.org/10.1006/jcph.1998.6010 . URL http://www.sciencedirect.com/ science/article/pii/S0021999198960107

Sengupta Tapan K., High accuracy computing methods: fluid flows and wave phenomena. New York, USA: Cambridge University Press 2013.

Sengupta T. K., Lakshmanan V. and Vijay VVSN., A new combined stable and dispersion relation preserving compact scheme for non-periodic problems. J Comput Phys 2009 228(8) 3048-3071. doi: 10.1016/j.jcp.2009.01.003.

Sengupta TK, Vijay VVSN, Bhaumik S. Further improvement and analysis of CCD scheme: dissipation discretization and de-aliasing properties. J Comput Phys 2009 228(17) 6150-6168. doi: 10.1016/j.jcp.2009.05.038 .

Sengupta T. K., Sengupta A. and Saurabh K., Global spectral analysis of multilevel time integration schemes: numerical properties for error analysis. Appl Math Comput 2017 304 341-357. http://dx.doi.org/10.1016/j.amc.2012.03.030. URL http://www.sciencedirect.com/science/article/pii/S0 09630 0312002627

Sengupta T. K., Ganeriwal G. and De S., Analysis of central and upwind compact schemes. J Comput Phys 2003 192(2) 677-94. http://dx.doi.org/10.1016/j.jcp.2003.07.015 . URL http://www.sciencedirect.com/science/article/pii/S0 0219991030 04133

Vichnevetsky R and Bowles J. Fourier analysis of numerical approximations of hyperbolic equations. Society for Industrial and Applied Mathematics; 1982. doi: 10.1137/1.9781611970876.

Sengupta T. K., Dipankar A. and Sagaut P., Error dynamics: Beyond von Neumann analysis. J Comput Phys 2007 226 1211-18. doi: 10.1016/j.jcp.2007.06.001.

Sengupta T. K. and Bhole A., Error dynamics of diffusion equation: effects of numerical diffusion and dispersive diffusion, J Comput Phys 2014 266 240-251. doi: 10.1016/j.jcp.2014.02.021.

Joshi V, Jaiman RK. A positivity preserving variational method for multi-dimensional convection-diffusion-reaction equation. J Comput Phys 2017 339 247-284. http://dx.doi.org/10.10 06/j.jcp.2017.03.0 05.

Sengupta T. K., Bhumkar Y. G., Rajpoot M. K., Suman V. K. and Saurabh S., Spurious waves in discrete computation of wave phenomena and flow problems. Appl Math Comput 2012;218(18):9035-9065. http://dx.doi.org/10.1016/j.amc.2012.03.030. URL http://www.sciencedirect.com/science/article/pii/S0 09630 0312002627.

Sengupta T. K , Jain R. and Dipankar A., A new flux-vector splitting compact finite volume scheme. J Comput Phys 2005 207 261-281.

Sousa E., Finite differences for the convection-diffusion equation: on stability and boundary conditions. Mathematical and Physical Sciences Division, University of Oxford; 2001. Ph.D. thesis . URL https://ora.ox.ac.uk/objects/uuid:8369da31- 2229- 4e05-846c- de3072ac1a37

Kwok Y-K., Stability analysis of six-point finite difference schemes for the constant coefficient convective-diffusion equation. Comput Math Appl 1992 23(12) 3-11. http://dx.doi.org/10.1016/0898-1221(92)90088-Y . URL http://www.sciencedirect.com/science/article/pii/089812219290088Y

Chan T. F., Stability analysis of finite difference schemes for the advection- diffusion equation. SIAM J Numer Anal 1984;21(2):272-284. doi:10.1137/0721020.

Wesseling P., von Neumann stability conditions for the convection-diffusion equation. IMA J Numer Anal 1996;16(4):583-598. doi: 10.1093/imanum/16.4.583 . http://imajna.oxfordjournals.org/content/16/4/583.full.pdf+html ; URL http: //imajna.oxfordjournals.org/content/16/4/583.abstract.

Christopher A. K. and Mark H. C, Additive Runge-Kutta Schemes for Convection-Diffusion-Reaction Equation, Combustion Research Facility, Sandia National Laboratories, Livermore, California (94551-0969), July 2001.

Blom J.G., and Verwer J.G., A comparison of integration methods for atmospheric transport-chemistry problems, Journal of Computational and Applied Mathematics 126 (2000) 381-396.

Verwer J.G., Sommeijer B.P., Hundsdorfer W., RKC time-stepping for advection-diffusion-reaction problems, Journal of Computational Physics 201 (2004) 61-79.

David L. R., John N. S., and Curtis C. O, Studies of the accuracy of time integration

methods for reaction-diffusion equations, Journal of Computational Physics 194 (2004) 544-574.

Anne B., Anita T. L., and Michael L. M., High-order multi-implicit spectral deferred correction methods for problems of reactive flow, Journal of Computational Physics 189 (2003) 651-675.

McRae G. J. and Seinfeld J. H., Numerical solution of the atmospheric diffusion equation for chemically reacting flows, J. Comput. Physics 45, (2000) 1-42.

Zhang Y., Bischof C. H., Easter R. C. and Wu T. T., Sensitivity analysis of mixed-phase chemical mechanism using automatic differentiation, J. Geophys. Res. 103 (D13) (1998) 18953-18979.

Yulong X. and Shu C., High-order finite volume WENO schemes for the shallow water equations with dry states, Advances in Water Resources 34 (2011) 1026-1038.

Chi-Wang Shu, Essentially Non-Oscillatory and Weighted Essentially Non-Oscillatory Schemes for Hyperbolic Conservation Laws, Institute for Computers and Application in Science and Engineering, NASA Langley Research Center, Hampton, VA, November 1997

Tian J. and Yong-Tao Z., Krylov implicit integration factor WENO methods for semilinear and fully nonlinear advection-diffusion-reaction equations, Journal of Computational Physics 253 (2013) 368-388.

Werner S. and Lee F. G., Oxygenation of ferrous iron, American Chemical Society,1961, 53, 143–146.

Ayora C., Manuel A. C., Francisco M., Tobias S. R., Jesus C. and Jose-Miguel N., Acid mine drainage in the Iberian Pyrite Belt: 2. Lessons learned from recent passive remediation experiences, Environ Sci Pollut Res, 2013, DOI 10.1007/s11356-013-1479-2

Plummer L. N. and Wigley T. M. and Parkhurst D. L., The kinetics of calcite dissolution in $CO_2-$ water systems at $5^oC$ to $60^oC$ and 0.0 to 1.0 atm $CO_2$, American Journal of Science, 1978, 278, 179–216.

Reddy M. M. and Plummer L. N. and Busenberg E., Crystal growth of calcite from calcium bicarbonate solution at constant $P_{CO_2}$ and $25^oC$ : a test of calcite dissolution model,Geochimica et Cosmochimica, 1981,45, 1281–1289.

Amikiya A. E. and Mapundi B., A stoichiometric method for reducing simulation cost of chemical kinetic models, Computers & Chemical Engineering 112 https://doi.org/10.1016/j.compchemeng.2018.02.020

Johnson R. S., A Modern Introduction to the Mathematical Theory of Water Waves, Cambridge University Press, Cambridge CB2 2RU, United Kingdom, 40 West 20th Street, New York, NY 10011-4211, USA 10 Stamford Road, Oakleigh, Melbourne 3166, Australia 1997, ISBN 0 521 59172 4

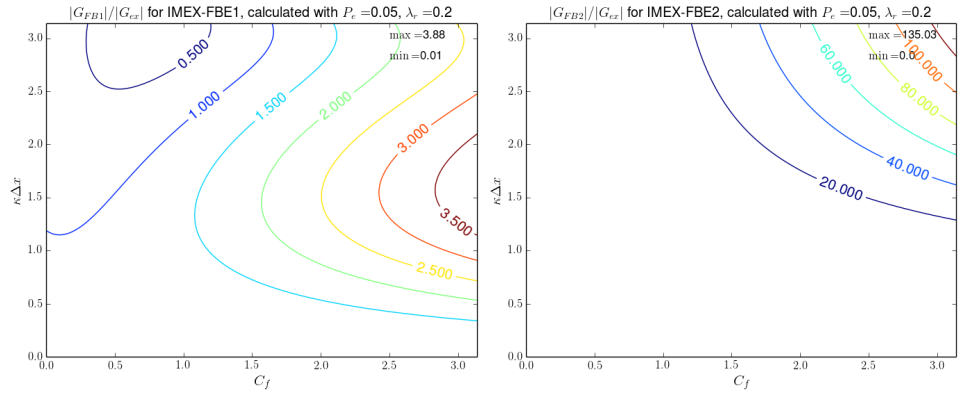


(a) IMEX-FBE1/diffusion-production model (b) IMEX-FBE2/diffusion-production model

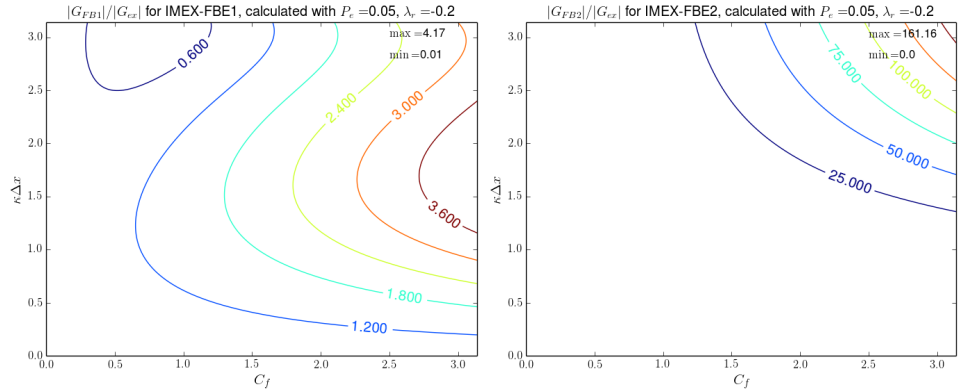


(c) IMEX-FBE1/diffusion-destruction model (d) IMEX-FBE2/diffusion-destruction model

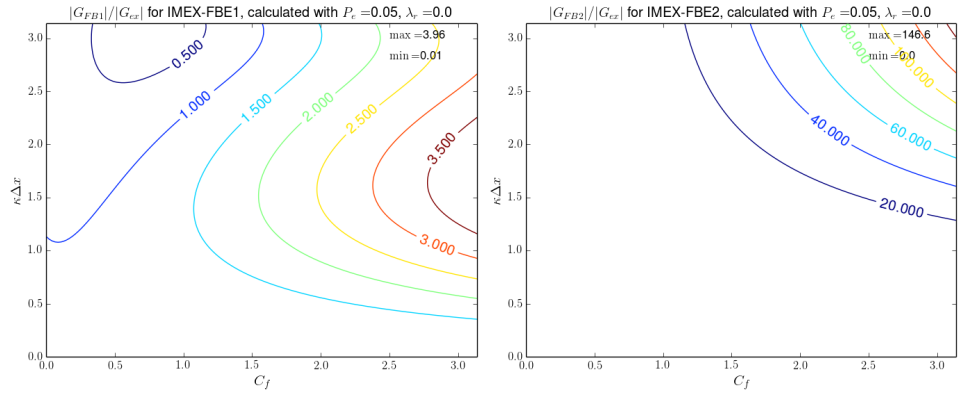


(e) IMEX-FBE1/non-reactive case model (f) IMEX-FBE2/non-reactive model

Figure 1: Contours of normalised amplification factors for IMEX-FBE1 and IMEX-FBE2 methods, obtained using $P_e = 0.05$. The bottom, middle and top rows display non-reactive, diffusion-destruction and diffusion-production cases of the 1D linear advection-diffusion-reaction equation, respectively.

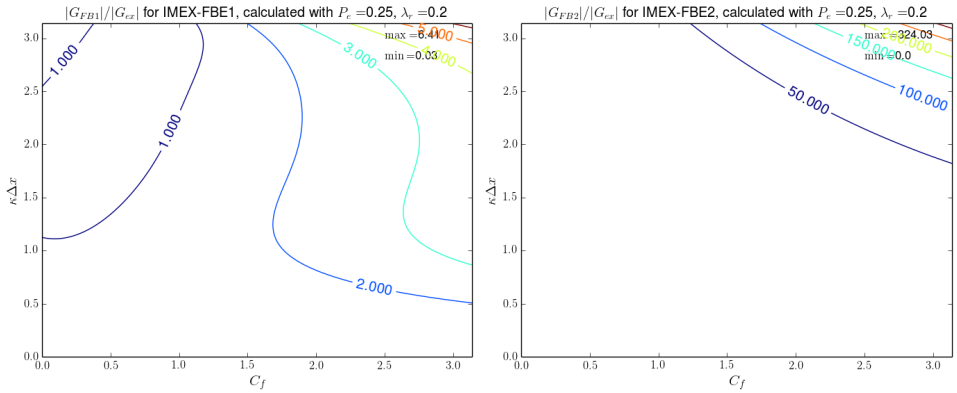


(a) IMEX-FBE1/diffusion-production model (b) IMEX-FBE2/diffusion-production model

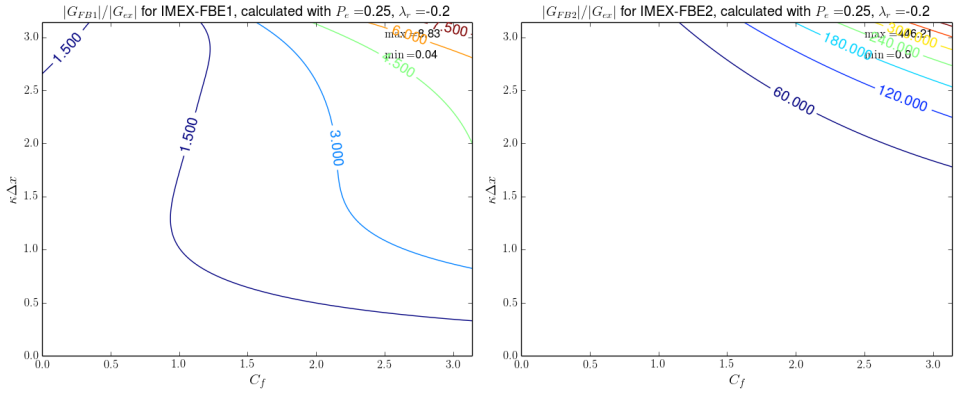


(c) IMEX-FBE1/diffusion-destruction model (d) IMEX-FBE2/diffusion-destruction model

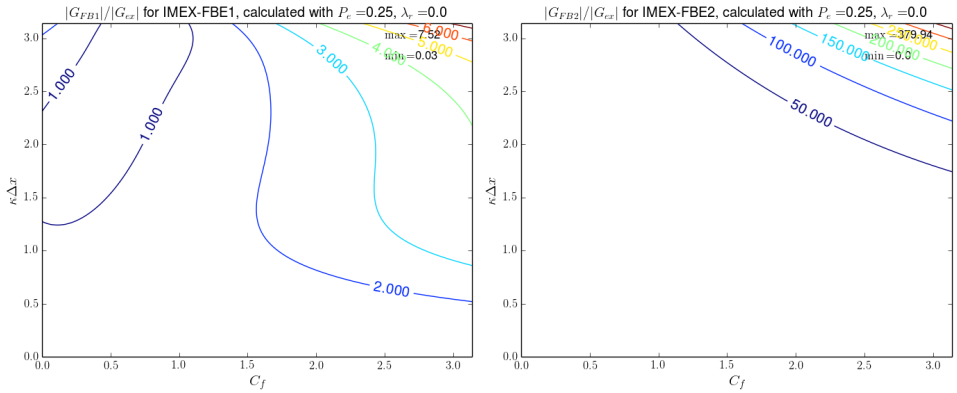


(e) IMEX-FBE1/non-reactive model (f) IMEX-FBE2/non-reactive model

Figure 2: Contours of normalised amplification factors for IMEX-FBE1 and IMEX-FBE2 methods, obtained using $P_e = 0.25$. The bottom, middle and top rows display non-reactive, diffusion-destruction and diffusion-production of the 1D linear advection-diffusion-reaction equation, respectively.

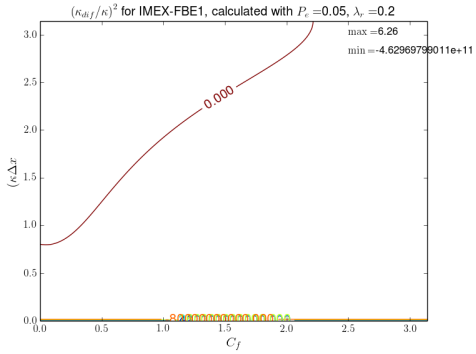


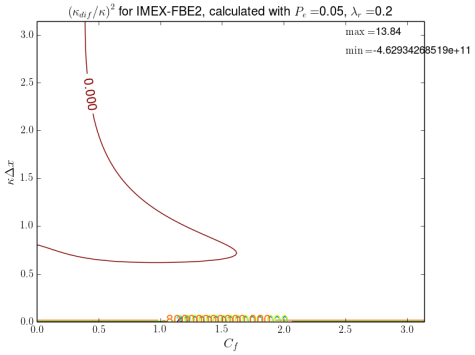


(a) IMEX-FBE1/diffusion-production model(b) IMEX-FBE2/diffusion-production model

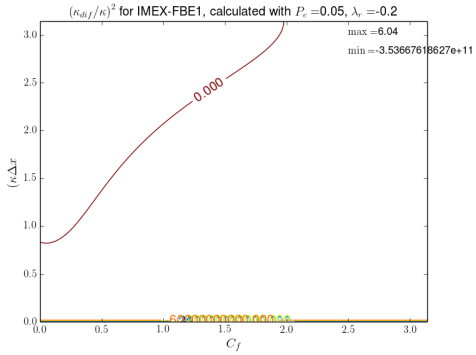


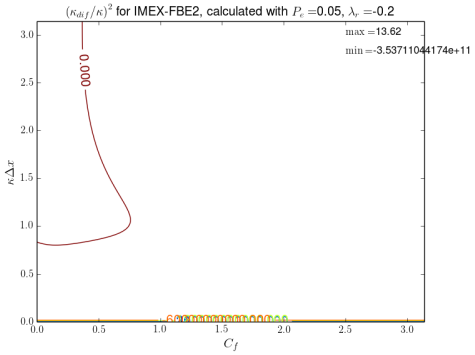


(c) IMEX-FBE1/diffusion-destruction model(d) IMEX-FBE2/diffusion-destruction model

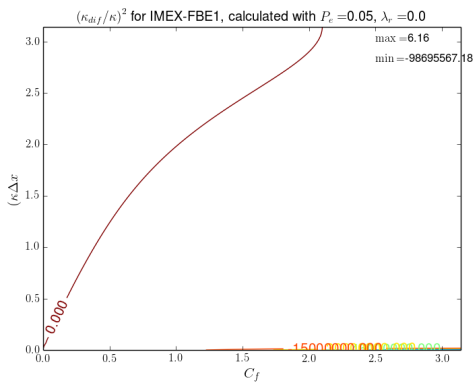


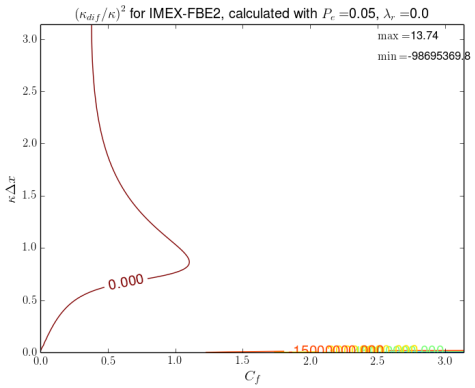


(e) IMEX-FBE1/non-reactive case model (f) IMEX-FBE2/non-reactive model

Figure 3: Contours of normalised diffusion relation for IMEX-FBE1 and IMEX-FBE2 methods, obtained using $P_e = 0.05$. The bottom, middle and top rows display non-reactive, diffusion-destruction and diffusion production cases of the 1D linear advection-diffusion-reaction equation, respectively.

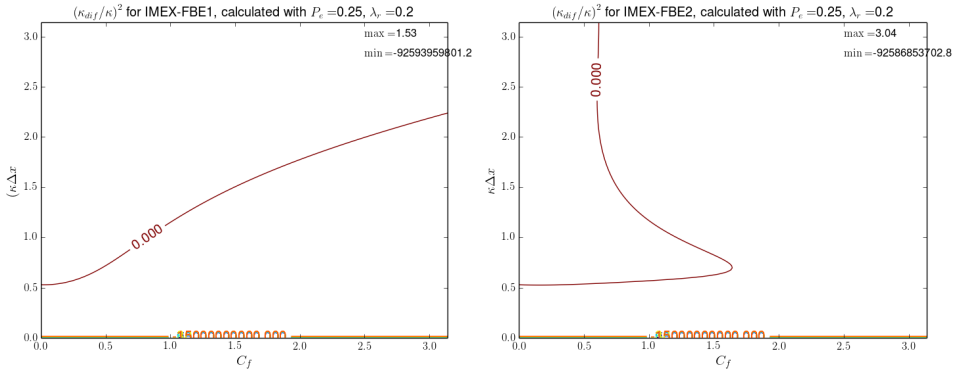


(a) IMEX-FBE1/diffusion-production model (b) IMEX-FBE2/diffusion-production model

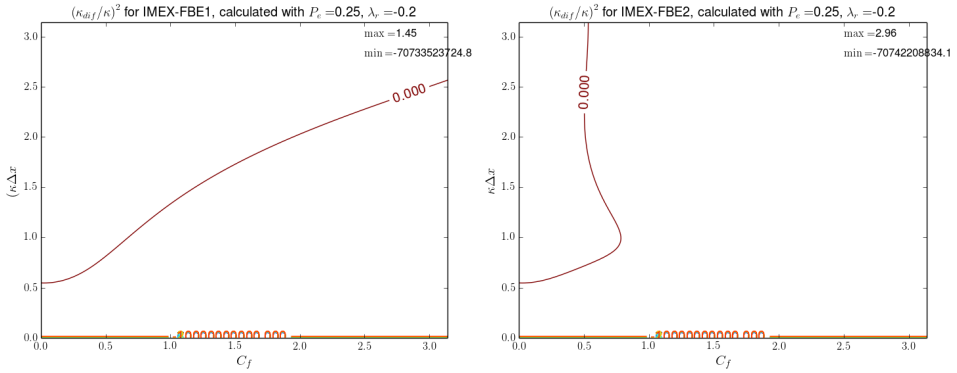


(c) IMEX-FBE1/diffusion-destruction model (d) IMEX-FBE2/diffusion-destruction model

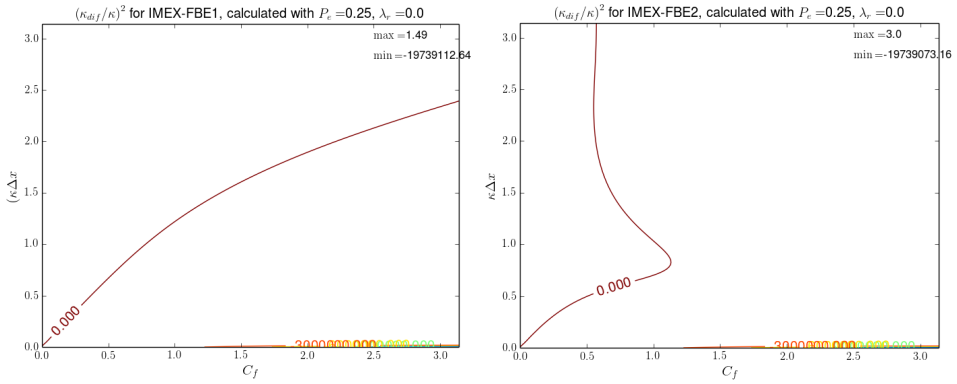


(e) IMEX-FBE1/non-reactive model (f) IMEX-FBE2/non-reactive model

Figure 4: Contours of normalised diffusion relation for IMEX-FBE1 and IMEX-FBE2 methods, obtained using $P_e = 0.25$. The bottom, middle and top rows display non-reactive, diffusion-destruction and diffusion production of the 1D linear advection-diffusion-reaction equation, respectively.

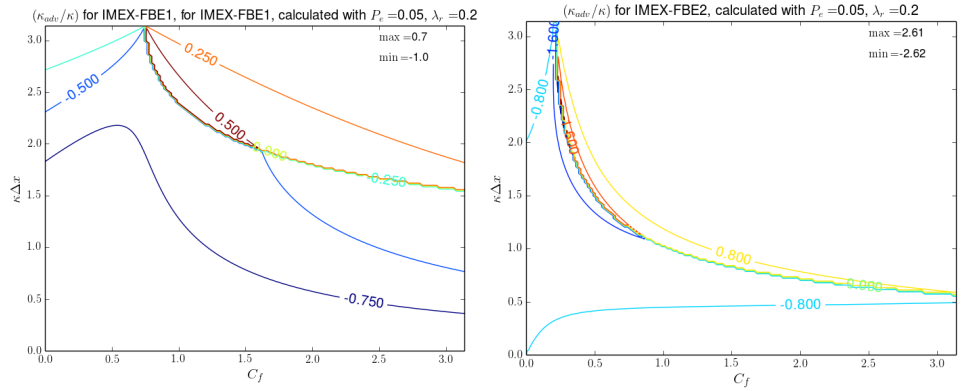


(a) IMEX-FBE1/diffusion-production model (b) IMEX-FBE2/diffusion-production model

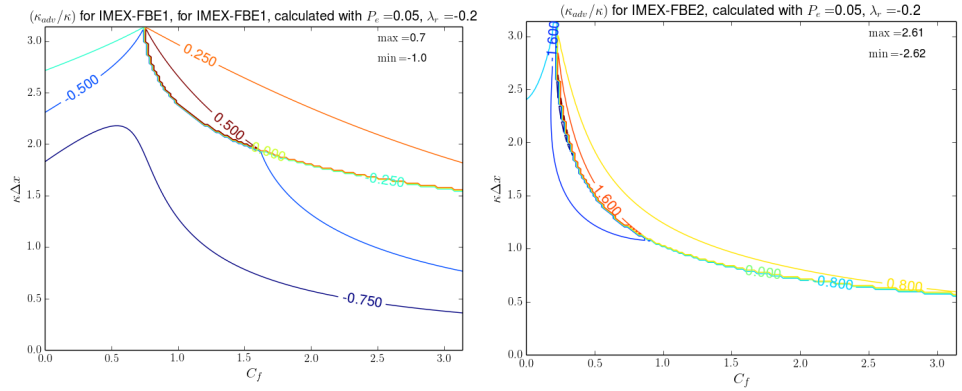


(c) IMEX-FBE1/diffusion-destruction model (d) IMEX-FBE2/diffusion-destruction model

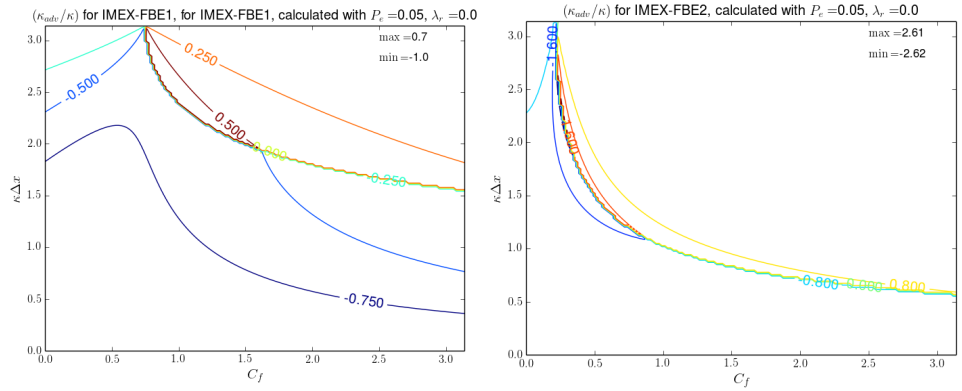


(e) IMEX-FBE1/non-reactive case model (f) IMEX-FBE2/non-reactive model

Figure 5: Contours of normalised advection wave numbers for IMEX-FBE1 and IMEX-FBE2 methods, obtained using $P_e = 0.05$. The bottom, middle and top rows display non-reactive, diffusion-destruction and diffusion production cases of the 1D linear advection-diffusion-reaction equation, respectively.

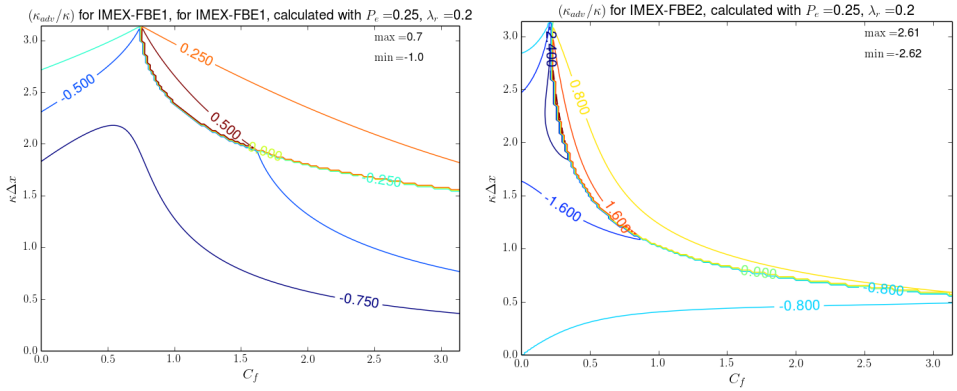


(a) IMEX-FBE1/diffusion-production model (b) IMEX-FBE2/diffusion-production model

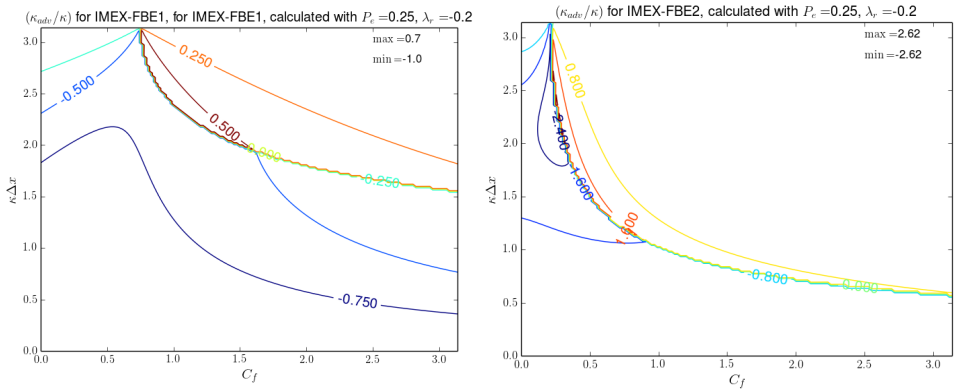


(c) IMEX-FBE1/diffusion-destruction model (d) IMEX-FBE2/diffusion-destruction model

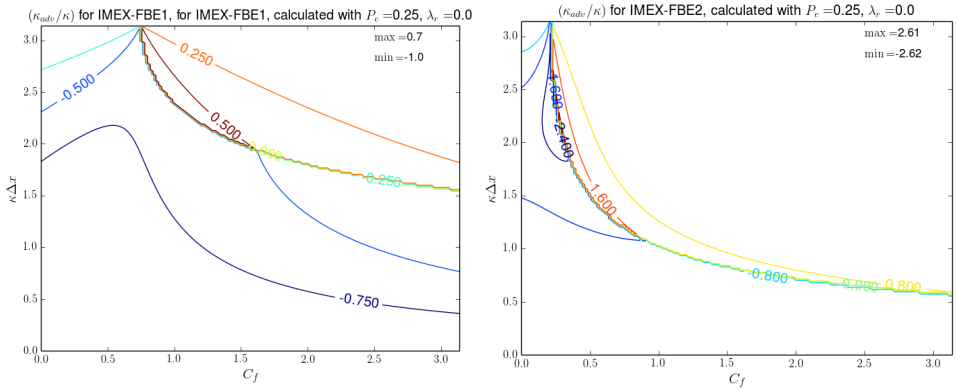


(e) IMEX-FBE1/non-reactive model (f) IMEX-FBE2/non-reactive model

Figure 6: Contours of normalised advection relation for IMEX-FBE1 and IMEX-FBE2 methods, obtained using $P_e = 0.25$. The bottom, middle and top rows display non-reactive, diffusion-destruction and diffusion-production of the 1D linear advection-diffusion-reaction equation, respectively.

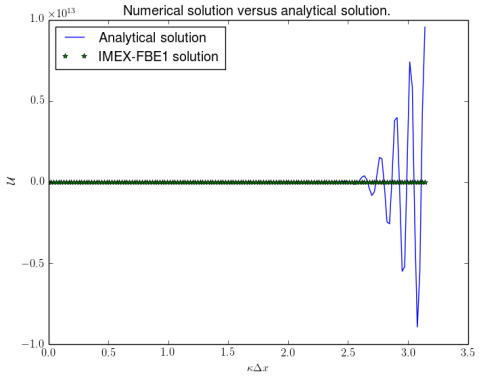


(a) IMEX-FBE1/diffusion-production model

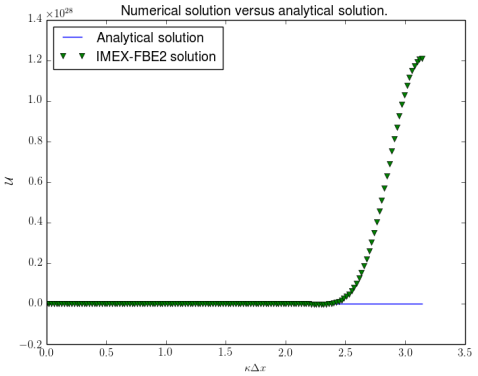


(b) IMEX-FBE2/diffusion-production model

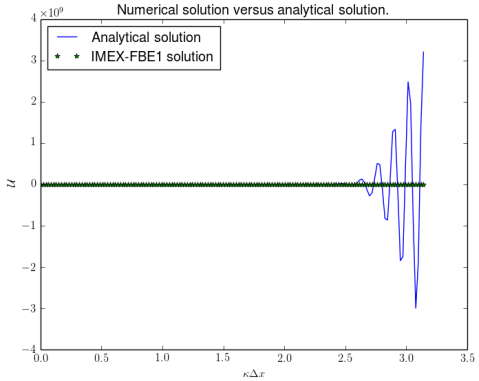


(c) IMEX-FBE1/diffusion-destruction model

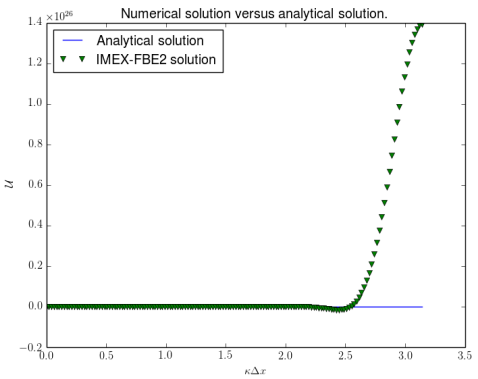


(d) IMEX-FBE2/diffusion-destruction model

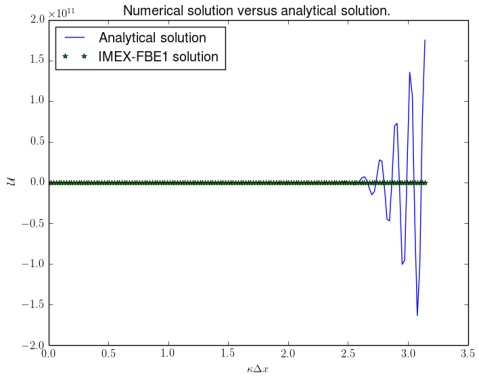


(e) IMEX-FBE1/non-reactive case model

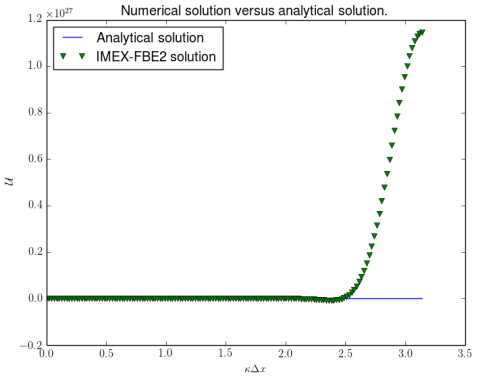


(f) IMEX-FBE2/non-reactive model

Figure 7: IMEX-FBE1 and IMEX-FBE2 solutions of the 1D linear convection-diffusion-reaction problem computed with $CFL = \frac{\pi}{2}$ and $P_e = 0.05$. The bottom, middle and top rows display non-reactive, diffusion-destruction and diffusion production, respectively.

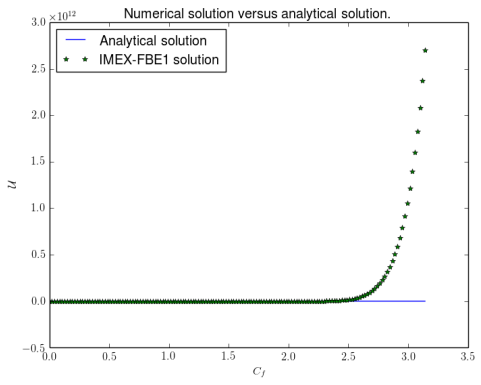


(a) IMEX-FBE1/diffusion-production model

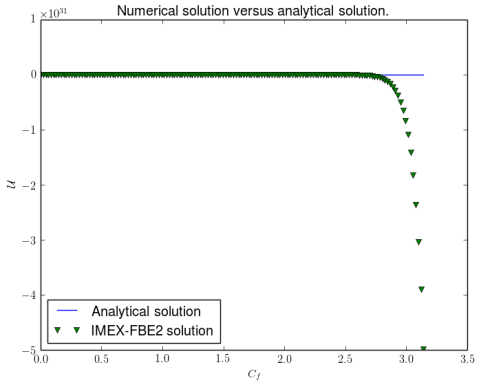


(b) IMEX-FBE2/diffusion-production model

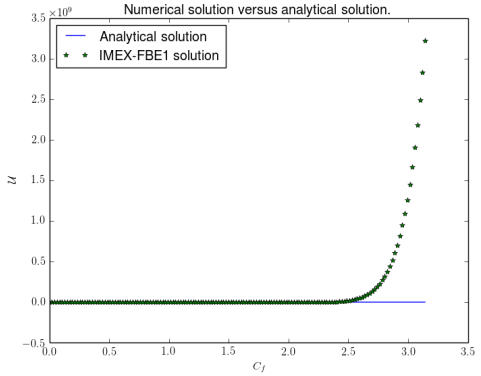


(c) IMEX-FBE1/diffusion-destruction model

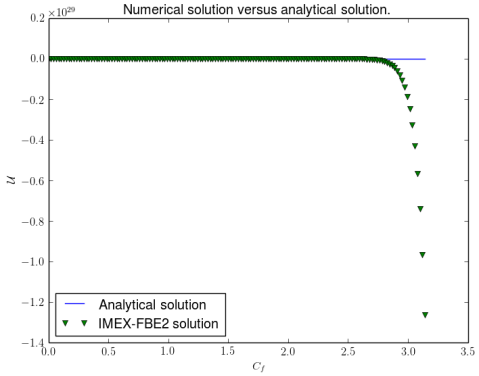


(d) IMEX-FBE2/diffusion-destruction model

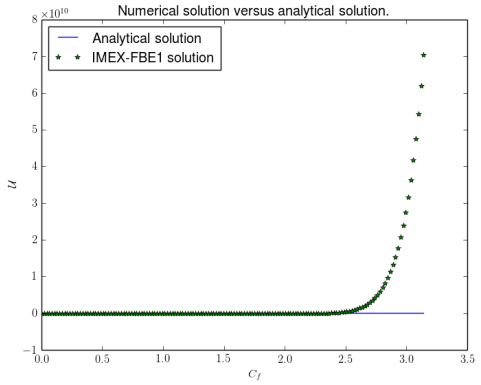


(e) IMEX-FBE1/non-reactive case model

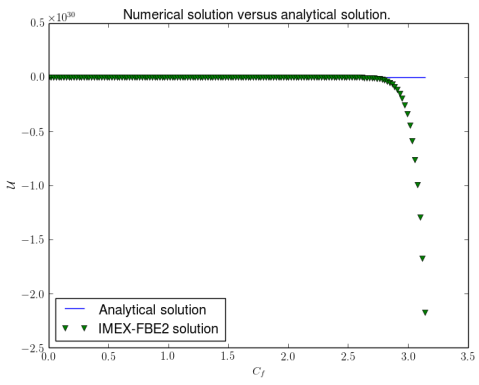


(f) IMEX-FBE2/non-reactive model

Figure 8: IMEX-FBE1 and IMEX-FBE2 solutions of the 1D linear convection-diffusion-reaction problem computed with $\kappa \Delta x = \frac{\pi}{2}$ and $P_e = 0.05$. The bottom, middle and top rows display non-reactive, diffusion-destruction and diffusion production, respectively.

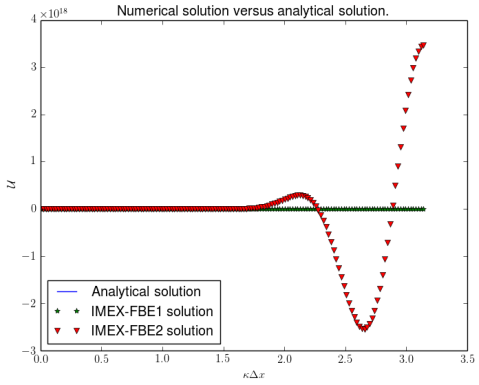


(a) IMEX-FBE1/diffusion-production model

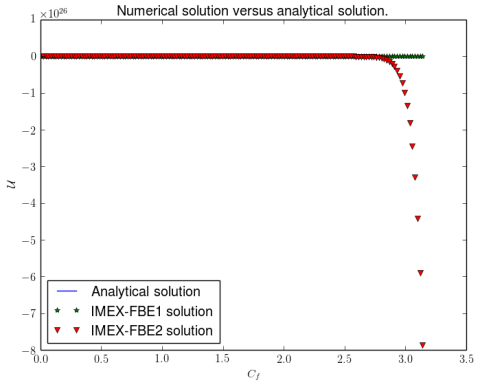


(b) IMEX-FBE2/diffusion-production model

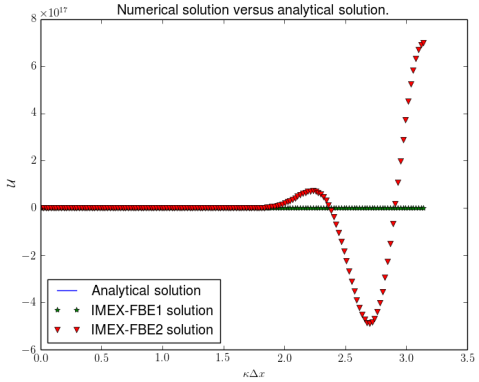


(c) IMEX-FBE1/diffusion-destruction model

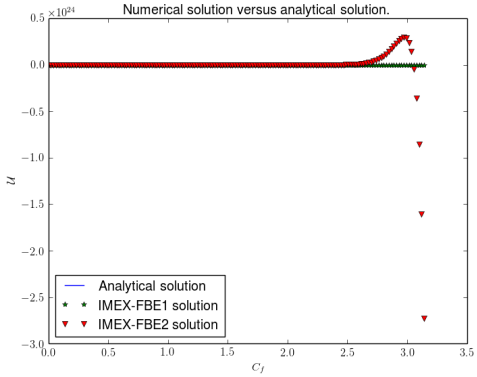


(d) IMEX-FBE2/diffusion-destruction model

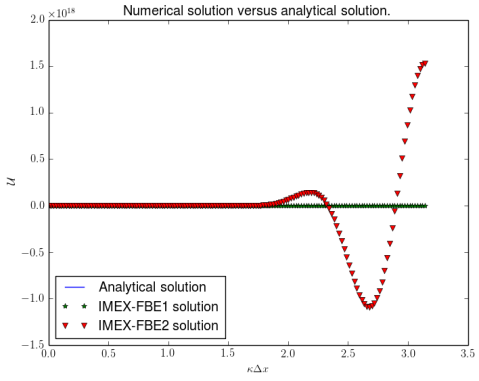


(e) IMEX-FBE1/non-reactive model

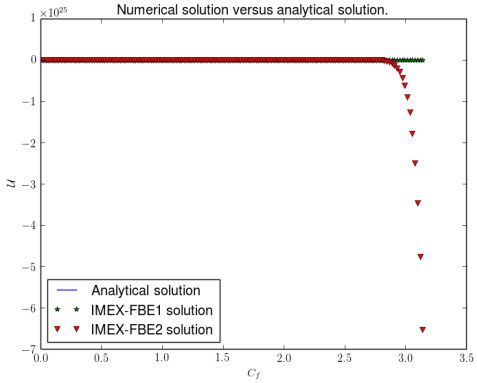


(f) IMEX-FBE2/non-reactive model

Figure 9: IMEX-FBE1 and IMEX-FBE2 solutions of the 1D linear convection-diffusion-reaction problem computed with $CFL = \frac{\pi}{2}$, $\kappa\Delta x = \frac{\pi}{2}$ and $P_e = 0.25$. The bottom, middle and top rows display non-reactive, diffusion-destruction and diffusion production, respectively.

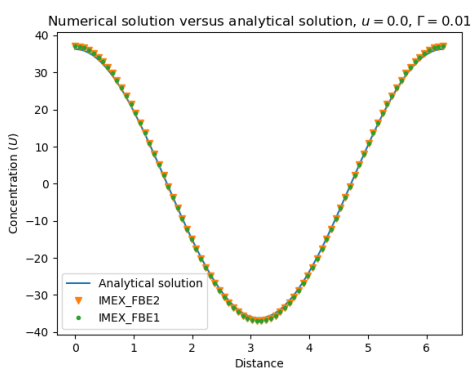


(a) Solutions/Diffusion transport

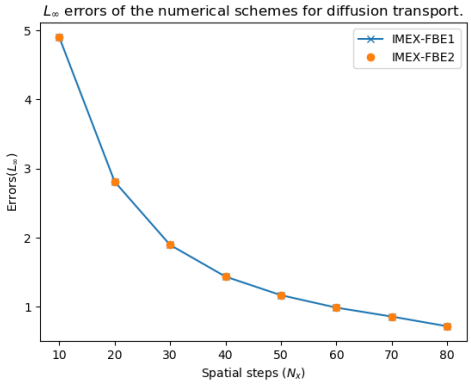


(b) $L_\infty$ error/diffusion transport

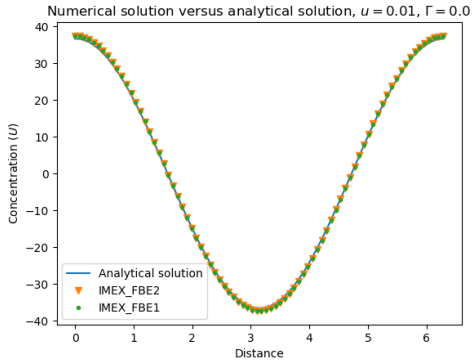


(c) Solutions/advective transport

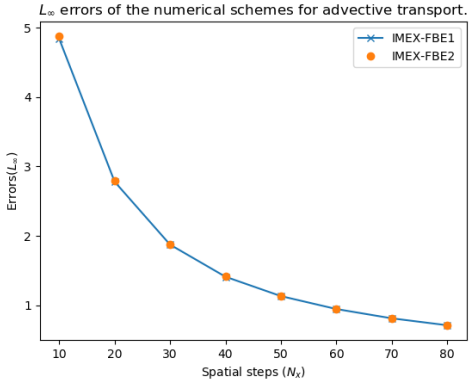


(d) $L_\infty$ error/advective transport

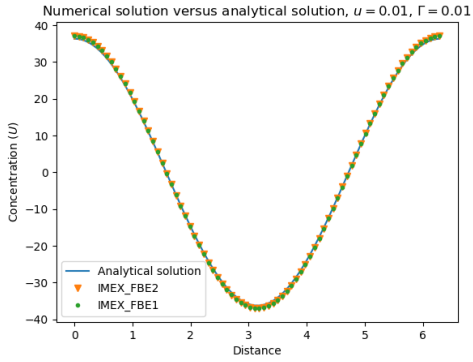


(e) Solution/advection-diffusion transport

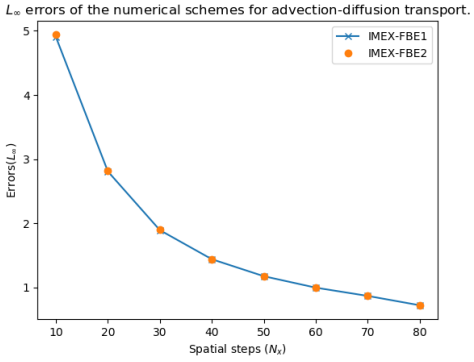


(f) $L_\infty$ error/advection-diffusion transport

Figure 10: Errors ($L_\infty$) and numerical solutions of the 1D stiff system (34)-(35), errors were computed using analytical solution (37). The solutions and errors were computed for diffusion dominated, advection dominated and semi-linear transport cases using $\Delta t = 0.5\Delta x$.

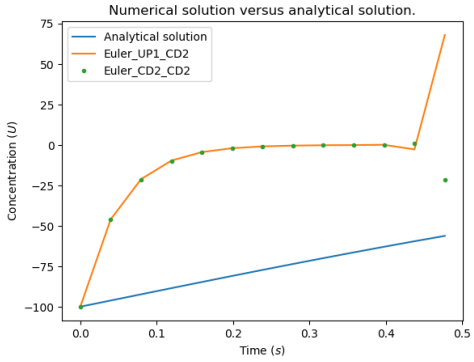


(a) Time/finite difference schemes

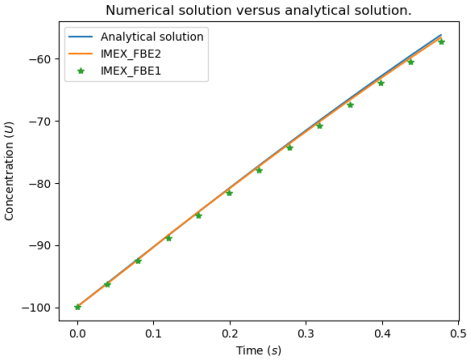


(b) Time/IMEX schemes

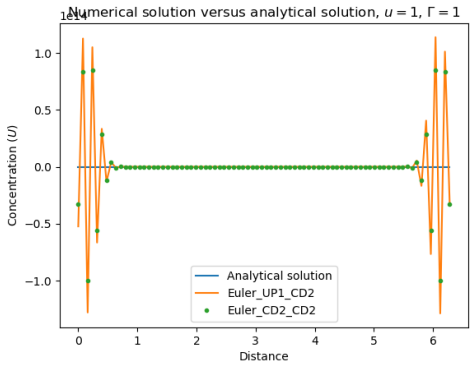


(c) Space/finite difference schemes

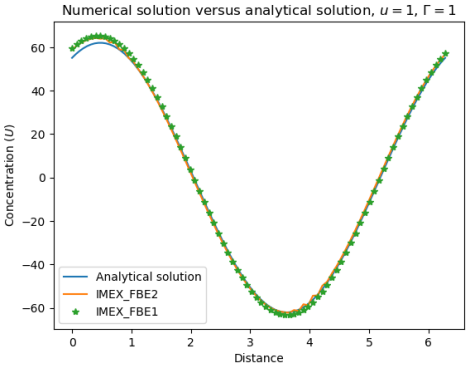


(d) Space/IMEX schemes

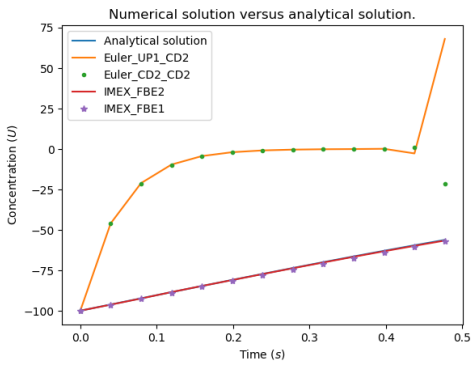


(e) Time/all schemes

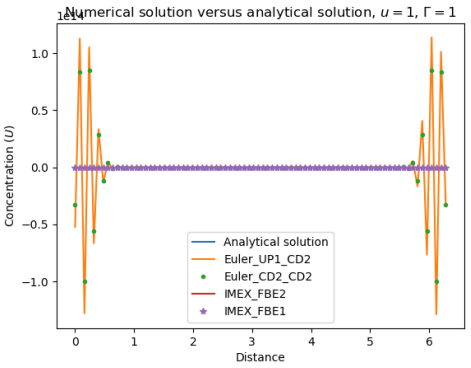


(f) Space/all schemes

Figure 11: Numerical and analytical solutions for the stiff system of semi-linear transport problem (34)-(35), computed with time step size $\Delta t = 0.5\Delta x$. The IMEX schemes are compared (in space and time) with finite difference schemes of the same order.

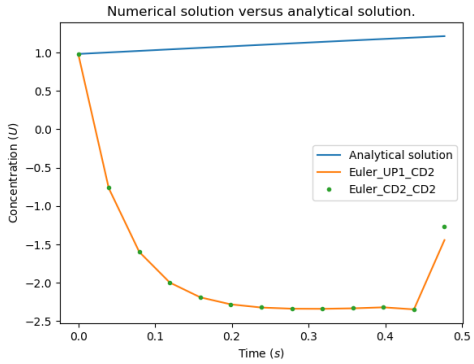


(a) Time/finite difference schemes

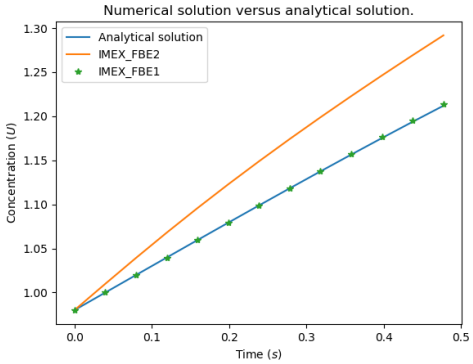


(b) Time/IMEX schemes

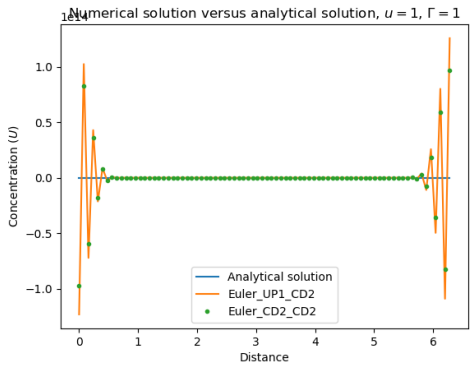


(c) Space/finite difference schemes

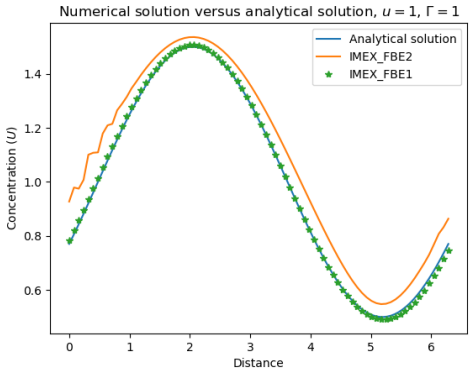


(d) Space/IMEX schemes

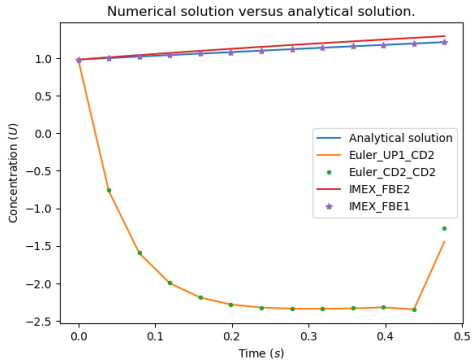


(e) Time/all schemes

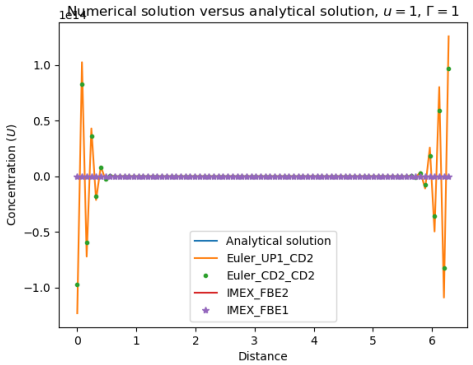


(f) Space/all schemes

Figure 12: Numerical and analytical solutions for the 1D stiff nonlinear transport problem (41)-(42), computed with time step size $\Delta t = 0.3\Delta x$. The IMEX schemes are compared (in space and time) with finite difference schemes of the same order.

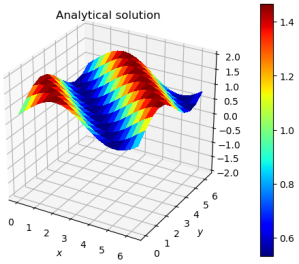


(a) Exact solution/nonlinear 2D problem

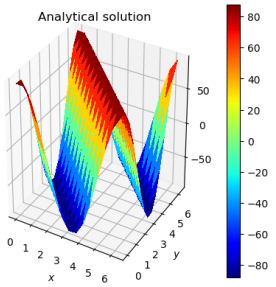


(b) Exact solution/stiff 2D linear system

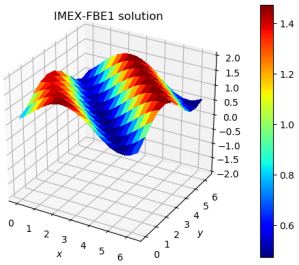


(c) IMEX-FBE1 /nonlinear 2D problem

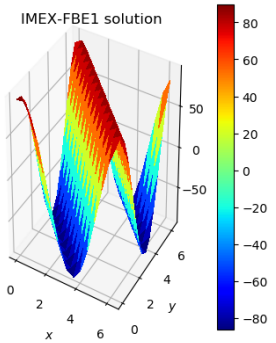


(d) IMEX-FBE1 /stiff 2D linear system

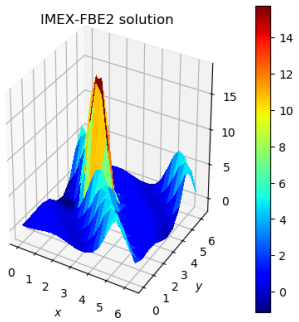


(e) IMEX-FBE2/nonlinear 2D problem

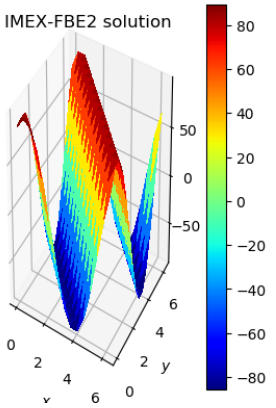


(f) IMEX-FBE2/stiff 2D linear system

Figure 13: Numerical and analytical solutions for the 2D system (43)-(44) and nonlinear transport problem (47), computed with time step size $\Delta t = 0.2\Delta x$. The right column represent solutions for the stiff system while the left column represent solutions for the nonlinear problem.

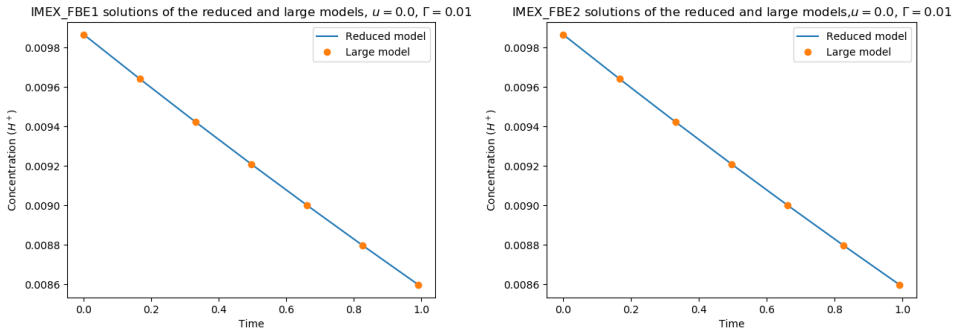


(a) IMEX-FBE1/diffusion transport (b) IMEX-FBE2/diffusion transport

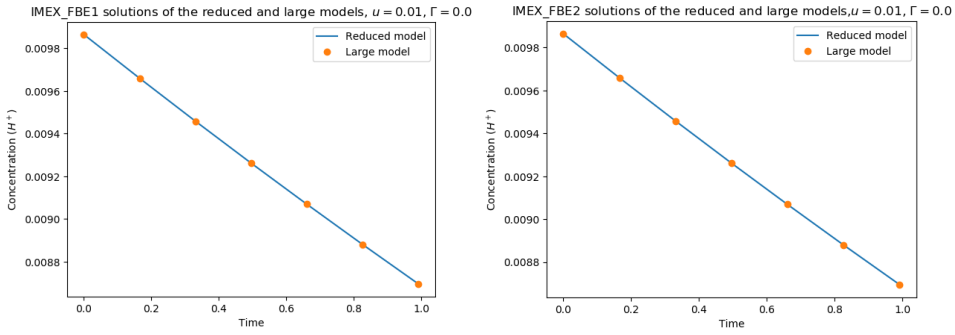


(c) IMEX-FBE1/advective transport (d) IMEX-FBE2/advective transport

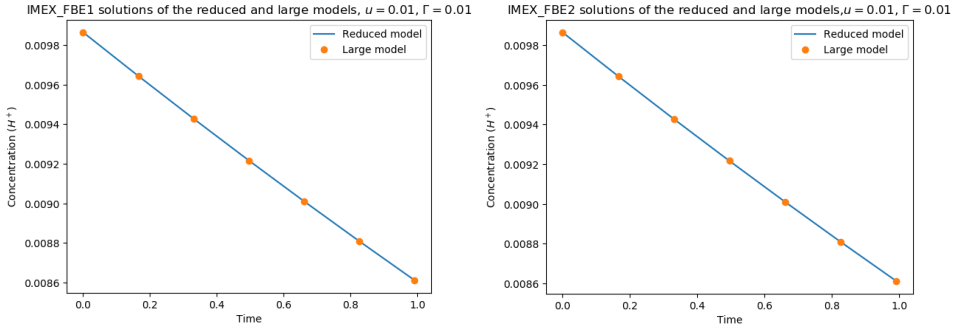


(e) IMEX-FBE1/advection-diffusion (f) IMEX-FBE2/advection-diffusion

Figure 14: IMEX-FBE1 and IMEX-FBE2 solutions of the acid drainage system

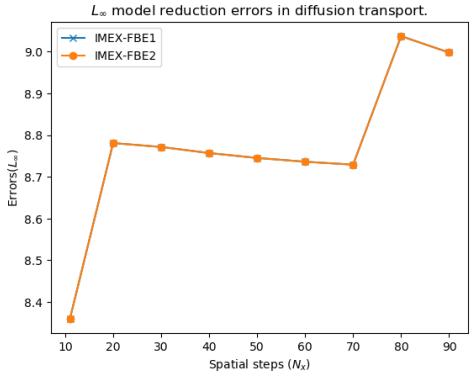


(a) $L_\infty$ errors/diffusion transport

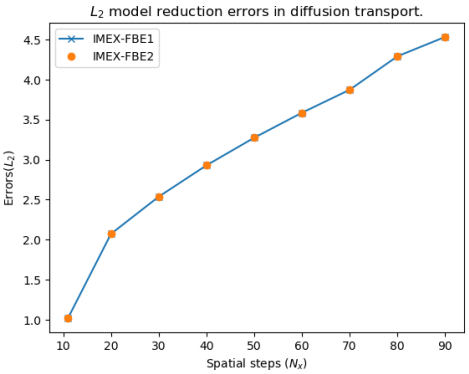


(b) $L_2$ errors/diffusion transport

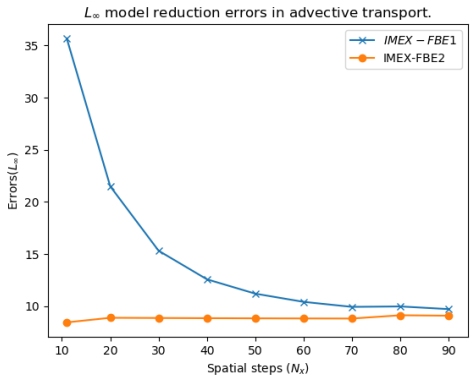


(c) $L_\infty$ errors/advective transport

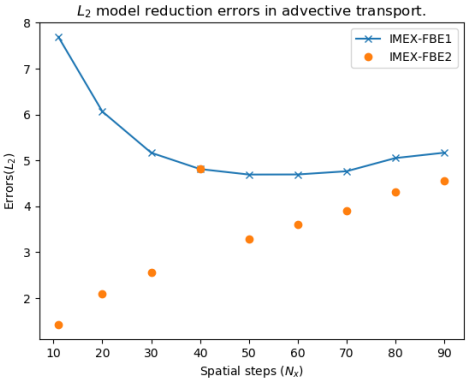


(d) $L_2$ error/advective transport

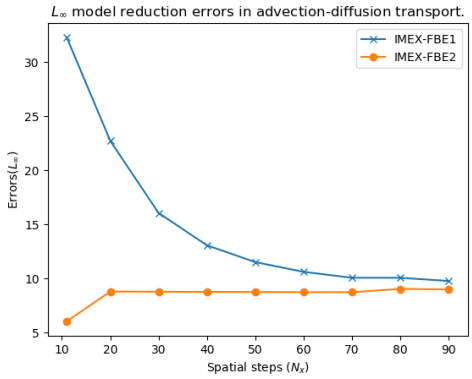


(e) $L_\infty$ errors/advection-diffusion transport

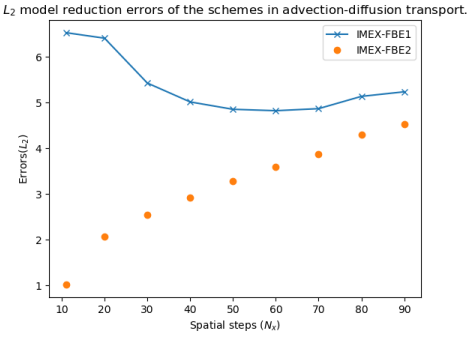


(f) $L_2$ errors/advection-diffusion transport

Figure 15: IMEX-FBE1 and IMEX-FBE2 solutions of the acid drainage system using 80 spatial steps.

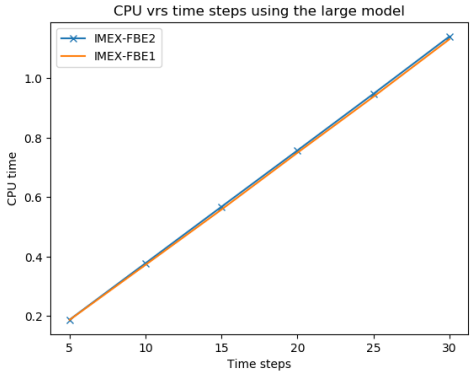


(a) CPU/large model/diffusion

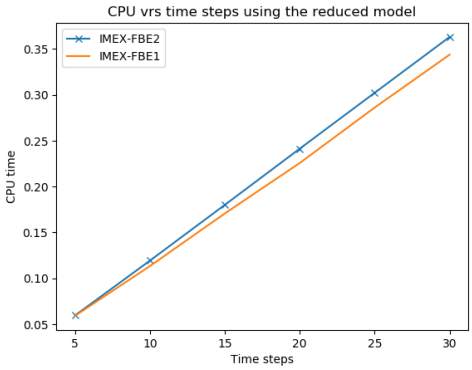


(b) CPU/reduced model/diffusion

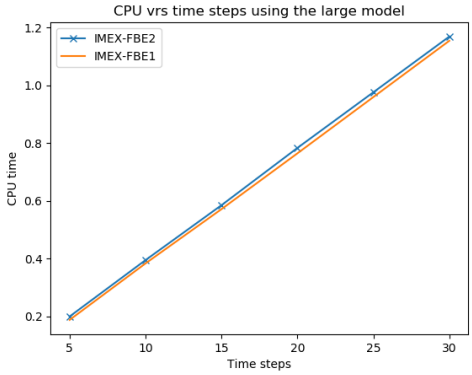


(c) CPU/large model/advection

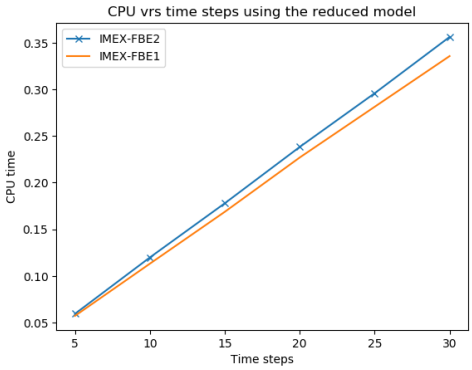


(d) CPU/reduced model/advection

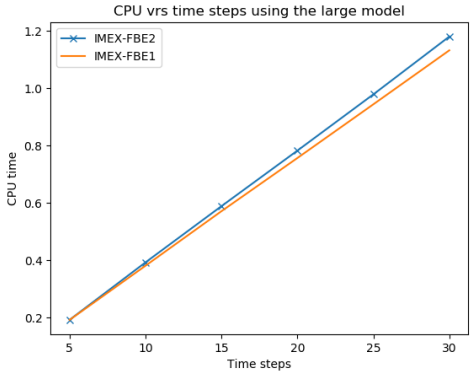


(e) CPU/large model/advection-diffusion

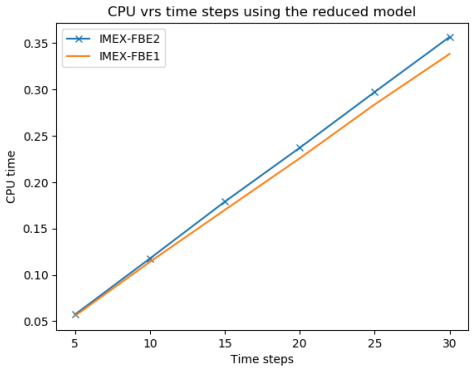


(f) CPU/reduced model/advection-diffusion

Figure 16: CPU time for IMEX-FBE1 and IMEX-FBE2 computed with 80 spatial steps in the acid drainage system